EXPERIMENTATION AND ANALYSIS OF COMPRESSION TEST METHODS FOR SINGLE FILAMENT HIGH PERFORMANCE FIBRES

THESIS

SUKRU FIDAN
1LT. TUAF
AFIT/GAE/AA/88D-14

DEPARTMENT OF THE AIR FORCE
AIR UNIVERSITY
AIR FORCE INSTITUTE OF TECHNOLOGY

Wright-Patterson Air Force Base, Ohio

AFIT/GAE/AA/88D-14

EXPERIMENTATION AND ANALYSIS OF COMPRESSION TEST METHODS FOR SINGLE FILAMENT HIGH PERFORMANCE FIBRES

THESIS

SUKRU FIDAN
1LT. TUAF
AFIT/GAE/AA/88D-14

AFIT/GAE/AA/88D-14

EXPERIMENTATION AND ANALYSIS OF COMPRESSION TEST METHODS FOR SINGLE FILAMENT HIGH PERFORMANCE FIBERS

THESIS

Presented to the Faculty of the School of Engineering

of the Air Force Institute of Technology

Air University

In Partial Fulfillment of the requirements for

the Degree of Master of Science

in

Aeronautical Engineering

Sukru FIDAN

1Lt., TUAF

December 1988

Acknowledgements

I would like to express my sincere gratitude to my thesis advisor Professor A. N. Palazotto, for his expert advice, guidance, motivation and great concern throughout this study. Also, I appreciate the support given by the Air Force Materials laboratories, Dr. W. W. Adams, who sponsored this thesis. My special thanks to Dr. S. Kumar, of the University of Dayton Research Institute (UDRI), for his guidance into the world of polymer science and for initiating the idea for this study. Also I would like to thank Gary Price, of UDRI, for his assistance in scanning electron microscopy, photo development, fixture preparation and other laboratory works.

Finally, I would like to thank the U.S. Air Force, granting me such a wonderful place of science and technology, AFIT.

Sukru Fidan

TABLE OF CONTENTS

LIST OF FIGURES

List of Tables

Abstract

The simple and reliable single filament test methods for predicting the compressive properties of fibers are a must for development activities of fibers in laboratories because of difficulties in composite compression test methods. Therefore, in this study, two single filament compression test methods, the elastic loop and bending beam tests, are conducted for several polymeric fibers including Kevlars, PBO and PBZT and a few carbon fibers such as T-50 and P-75S, in order to obtain their compressive properties. Also the compressive failure modes of fibers, which occur as a kink band formation in polymeric fibers and as a fracture in carbon fibers are investigated. In addition, a FORTRAN program is written for numerical analysis of non-linear geometry elastica problems such as bending of a single fiber considering large displacements.

A comparison of the results obtained in this study is made with previous studies. It is found that, generally,the compressive strengths of the fibers obtained from elastica loop and bending beam tests,are higher than the composite compression test results. The kink band formation in polymeric fibers were investigated and it can be concluded that the critical kink band formation represents the buckling of separated microfibrils due to

elastic instability. Also the FORTRAN program is applied to measure the fiber compressive properties as a new potential single filament test method.

EXPERIMENTATION AND ANALYSIS OF COMPRESSION TEST METHODS FOR SINGLE FILAMENT HIGH PERFORMANCE FIBERS

CHAPTER I

1. INTRODUCTION

1.1 Problem

High performance polymeric fibers are main reinforcement for composite materials. Although these composites show excellent tensile properties, their behavior under compression is very poor. For instance, Du Pont's Kevlar™ are used to replace glass fibers in many applications due to their higher modulus and mechanical properties, but they are not satisfactory for replacements for graphite fibers in critical applications such as primary aircraft structures because of their lower compressive strengths. A study showed that Kevlar fiber-reinforced composites exhibit longitudinal compressive strengths which are only less than 20 % of their longitudinal tensile strengths [1]. Another study indicated that the compressive failure of Kevlar 49 composites is not due to the matrix material, but it is due to the very low compressive yield strength of the Kevlar 49 fibers themselves.

There is no clear explanation of compressive failure mechanisms in polymeric fibers. The only way to understand

their compressive failure modes and behaviors under compression is the single filament compression test. Actual composite testing is not feasible in developing programs of fibers, because the limited number of sample fibers are produced in laboratories. Compression testing of composites in itself is not straight forward because of the sample preparation, alignment, testing methodology, etc. Therefore small quantity or single fiber test methods are needed.

1.2 Purpose of Study

Towards the solution of the problem explained above, this study investigates the following objectives:

1. The reliability and validity of two compression test methods. These are: Elastica loop test and bending beam test.

2. To obtain the compressive properties of high performance polymeric and some carbon fibers.

3. Microstructural observations related to the behavior of fibers under compression, namely, kink band formation and fibril microbuckling.

4. Nonlinear numerical analysis of elastica problems such as bending of a fiber considering large displacements.

1.3 Background

General properties of polymeric and carbon fibers, fiber compressive failure modes, kink band formation, fiber morphology and compressive test methods will be discussed in detail in Chapter II.

1.4 Previous Studies

Elastica Loop test

David Sinclair, in 1950, measured the tensile strength and Young's modulus of glass fibers by pulling the fibers into a loop until it breaks [3]. He indicated that the looped fiber is equivalent to a very short straight fiber since the loop fiber is strained to its breaking point over a very short length of 1 mm or less. He calculated the minimum radius of curvature at any point in the looped fiber by using elastica equations derived by assuming that the fiber is a linear elastic bar.

In 1970, W. R. Jones and others considered intrinsic strength and non-Hookean behavior of carbon fibers by using the elastica loop test [4]. They found out that the strains obtained in this experiment are much higher than those observed for 1-in. gauge lengths in tension by a factor of two or three.

In 1980, M. G. Dobb and others studied the compression deformation of Kevlar fibers by using the elastica loop test and scanning and transmission electron microscopes. They proposed a structural mechanism describing the mode of deformation based on the initial formation of kink bands.

Allen S. R. [6], in 1983, studied bending and compressive behavior of PBZT (poly paraphenylene benzobisthiazole) and PPTA (poly paraphenylene terephathalamide) fibers by using the elastica loop test. He

found out that the curvature contributions due to shear and material anisotropy are negligible. He also observed that the onset of kinking due to compressive stresses precludes the attainment of a tensile failure in the loop which is more common for brittle materials.

S. van der Zwaag and G. Kampschoe [7] studied the compression strength of aramid fibers. They used the elastica loop test to calculate the compressive strength of fibers by assuming that the kink bands at the bottom of the loop act as plastic hinges, and by using simple elastic bending beam theory equations. They found out that the compression strength of aramid fibers is a function of elastic modulus, but not the tensile strength.

Bending Beam Test

In 1985, S. J. DeTerasa [8] studied the compressive failure mechanisms of polymer fibers by using the bending beam test which permits the applications of small, measurable axial compressive strains to initiate kink bands in the fibers. He proposed the concepts of compressive failure mechanisms in fibers due to elastic microbuckling instabilities in axially compressed extended-chain polymers. He also correlated that the compressive strength of five polymeric and carbon fibers is approximately equal to one-third of their longitudinal shear modulus.

Kink Band Formation

Kink band formation concept is very important because it is a compressive failure mode in polymeric fibers. Many workers studied this subject. DeTerasa [8] stated that the critical compressive stress that initiates local buckling instabilities which subsequently lead to kink band formation in anisotropic materials is the compressive strength of these materials.

First, in 1962, the kink bands were described by Orowan [8] as the deformation bands that result from the cooperative buckling of the easy shear slip planes. Orowan's theory was later used by DeTerasa to form a concept of kink band formation mechanism in polymeric fibers.

Dobb and others, in 1980, explained the phases of kink band formation [5]. Zwaag et al. [11] studied kink band formation in aramid fibers. They measured the kink band formation in single aramid filaments as a function of the applied compressive strain.

Also kink band formation has been observed in many compressed anisotropic materials such as reinforced composites [9,2,10] and woods [8].

Numerical Analysis of Elastica Problems

Miller [23] studied the numerical analysis of elastica problems such as a planar, continuous, flexible member by using the shooting method and Newton-type iteration.

1.5 Thesis Presentation

Chapter I gives an introductory explanatic of the problem and the purpose of this study. Also previous studies are given in this section.

Chapter II deals with the background of the subject, such as general properties of polymeric and carbon fibers, fiber compressive failure modes, fiber morphology and compressive test methods.

The experimental set-up and procedures are studied in Chapter III. This section also includes advantages and disadvantages of the test methods.

In Chapter IV, the results and observations are discussed. Besides the general comparison of compressive strength of the fibers studied, each fiber's compressive behavior is discussed separately.

Chapter V gives conclusions and recommendations.

The appendix section includes a potentially new compressive test method, called the elastica shooting test, which applies nonlinear numerical analysis of elastica problems such as bending of a fiber with large displacements. This section also includes a FORTRAN code and a test equipment list.

CHAPTER II

2. BACKGROUND

2.1 High Performance Organic Fibers

In this study, the bending beam tests and elastica loop tests have been conducted, mainly on polymeric fibers, but also on a few carbon fiber for comparison of the failure modes. Therefore, a basic understanding of fibers' structure is explained in the next two sections in order that the reader can appreciate the micromechanical characteristics of the fibers investigated.

Polymeric Fibers

Polymers consist of long, covalently bonded molecular chains in which molecules are made up of repeating chemical units. These molecules are produced through the process of polymerization.

Polymers' high mechanical properties such as high tensile strength and stiffness originate from the covalent bonds of long chain molecules, oriented along the fiber axis. These chains are intermolecularly bonded by weak van der Walls or hydrogen bonding. These lateral interactions between chains are weak compared to the strength of the covalent bonds along the chain, by a factor of 10 to 100 [12]. This leads to a very anisotropic fiber with low compressive strength and low shear modulus.

High-performance polymeric fibers are classified into two groups [12]: Extended chain flexible polymers and liquid crystalline polymers. There are two major types of liquid crystalline polymers; thermotropic polymers, which are melt processed and lyotropic polymers, which are processed in solution. In this study, liquid crystalline-solution spinning-lyotropic-polymers such as Kevlar™ (poly paraphenylene terephathalamide or PPTA), PBZT (poly paraphenylene benzobisthiazole) and PBO (poly paraphenylene benzobisoxazole) are examined. Their morphologies are explained in detail in the fiber morphology section.

Carbon Fibers

The carbon (graphite) fibers have high mechanical properties because of the structure and orientations of the carbon crystals. Planar layers of carbon atoms stack on top of each other in graphite crystal. Within these layers, which are oriented along the fiber axis, the carbon atoms are joined by strong covalent bonds [13].

Although, the atoms in the layer are held together by very strong covalent bonds, weak van der Walls forces interact between layers. This means that the fiber is highly anisotropic [14].

The high modulus carbon fibers have fibrillar/microfibrillar morphology. Carbon fibers have brittle or shear fracture in compression, whereas polymeric

fibers show kink band formation under compressive stresses [15].

2.2 Fiber Compressive Failure Modes

Fiber compressive failure modes can be classified into three groups: shear failure which is dominant in high modulus carbon fibers; kink band formation which is mostly seen in polymer fibers and the bending failure of brittle fibers, such as glass fibers. Although the bending failure starts on the tension side, kink band formation starts at the compression side. The shear failure occurs along a maximum shear plane.

Since this thesis studies mostly polymeric fibers, kink band formation will be discussedin detail in the next section.

Kink Band Formation

If we consider uniaxial compressive failure for isotropic and anisotropic materials; we see that although isotropic materials slip plastically or fracture along the planes at 45 degrees to the load direction, the mechanism of compressive failure in anisotropic planes depends on material symmetry (orientation of easy shear slip planes) and direction of compressive load with respect to this symmetry. The compressive stress which is required to slip these planes [8] is:

$$\sigma = \frac{\tau_c}{\cos\theta \sin\psi}$$

where τ_c = critical shear stress.

θ = orientation of normal to slip plane with respect to compressive load axis.

ψ = orientation of slip direction with respect to compressive load axis.

As DeTerasa stated [8], in anisotropic materials, kink bands are formed when the compression stress is applied parallel to material planes of easy shear slip that are much larger than the atomic scale. Also, he proposed the stages of axial compressive failure due to the kink band formation in fibers as follows:

. The initiation of local elastic instability in the fiber occurs when the critical axial compressive stress equals the minimum longitudinal shear modulus of the fiber.

. This critical stress causes elastic buckling deformation which results in shear slip between the planes of easy shear slip. (i.e. between chains and microfibrils in the fiber.)

. Instability propagates through the fiber when this shear failure eliminates the elastic foundation between chains or microfibrils.

. Buckled material collapses to the observed angular

kink band due to severe bending at the kink band boundaries.

DeTerasa studied the comparison of compressive behaviors of Kevlar™ 49 and wood, stating that, both have a material structure with cylindrically orthotropic symmetry. He concluded that formation of compressive kink bands within particular planes of orthotropic materials results from shearing between the buckled planes (not necessarily crystallographic planes) of the easy shear slip. Also he proposed that this compressive failure mechanism might be universal for orthotropic materials.

Dobb et al. [5] stated a compressive failure model in Kevlar™ fibers parallel to the above ideas. They proposed that, in the Kevlar™ fibers, a low compressive stress could be expected to initiate shear between, or delamination of adjacent chains or microfibrils as a result of low lateral strength arising from relatively weak van der Wall forces and the oriented hydrogen bonding between chains or microfibrils.

In this thesis, the above fiber compressive failure proposals are considered carefully. It is believed that the compressive stress is just enough for the initiation of local elastic instabilities which, subsequently, leads to critical kink band formation in anisotropic fibers, and this stress is the compressive strength of these fibers.

Some workers considered the fiber kink band formation as a result of the plastic deformation of the fibers on the molecular level [16,11]. Zwaag et al. [11] stated that

'kink bands are not elastic instability of fiber as a geometrical unit but are due to a plastic instability of the filament material.'

2.3 Fiber Morphology

This study would like to prove that the critical kink band formation is totally a result of elastic instability in polymeric fibers, which is seen as accumulation of very fine black lines through compressed fiber cross-section with a certain angle to the fiber axis. It is believed that this is because of collapsing of microbuckling regions of separated microfibrils from each other under compressive stresses. This section is intended to give the reader an idea about the structural model of ordered polymers.

In the article by Linda C. Sawyer [17], the morphology of aramids and ordered polymer fibers has been described by a hierarchical structural model which includes fibrillar textures. As seen in figure 1, the structural hierarchy of the fibers shows the fibrillar structure composed of macrofibrils (5000nm), fibrils (500nm) and microfibrils which are 50 nm wide and 5 nm thick.

As mentioned in this article, the first time, Dobb and the others observed 'hierarchies' of structure of the aramid fibers consisting of radially arranged sheets, regularly pleated along the fiber axis. They indicated that each sheet is composed of extended molecular chains connected laterally by hydrogen chains. Also, in the tangential

direction of the fiber there are weaker secondary bonds between chains or between sheet planes. This model, later, was used by DeTerasa in comparison to helical kink band formation in Kevlar™ 49 fiber and inwood under compression, knowing that both have cylindrically orthotropic material properties. (See the Section 4.3.2)

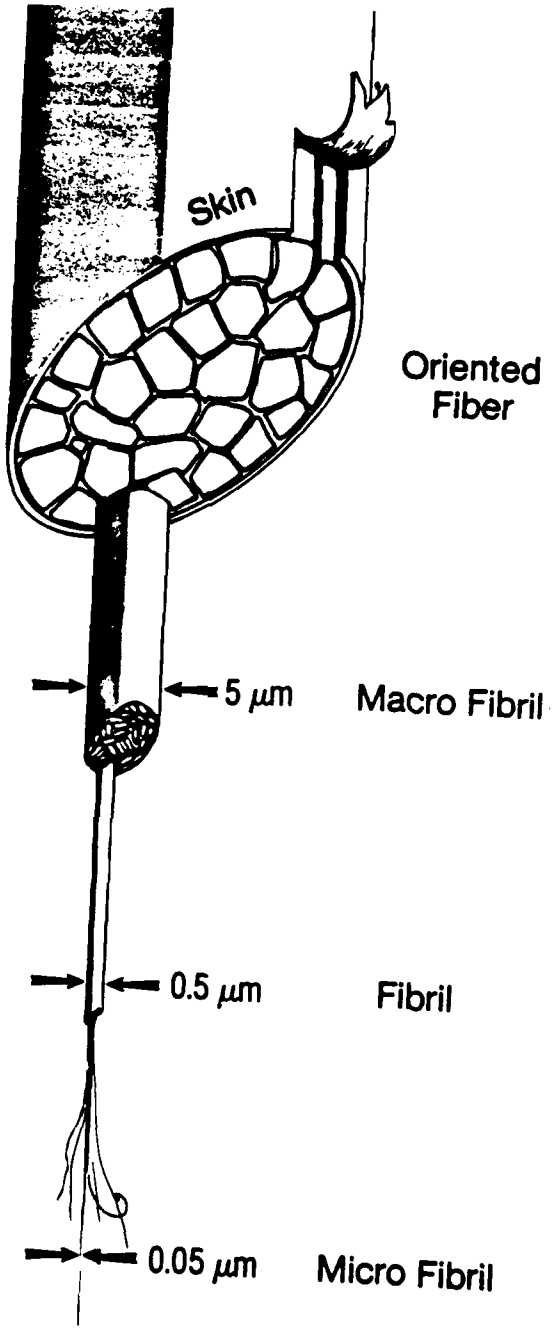

Figure 1. The Liquid Crystalline Polymers' Structural Model in a Schematic of the Fibrillar Structure Typical of Highly Oriented Materials. (After [17]).

2.4. Compressive Test Methods

Introduction

The investigation of compressive properties of high performance fibers is very important to their improvement studies. Therefore, many workers used different techniques to apply uniform axial compressive stresses to single fibers to obtain their compressive properties. Since the fiber diameter is very small (for example, about 13 μm for Kevlar™ fibers), applying true axial compression stresses to fiber itself is difficult without buckling. Hence, most of the techniques use a matrix material to support the fiber against buckling and to transmit uniform axial compressive stresses to the fiber such as bending beam test and embedding fibers in the matrix. Also there are two other distinct indirect techniques in literature for measuring the compressive properties of single fibers: elastica loop test and recoil test.Various compression tests used for fibers and composites are discussed below.

Bending Beam Test

This test was first used by DeTerasa [8] in his dissertation to investigate the modes of compressive failure and to predict the compressive strengths of high performance polymer fibers. In this technique, the fibers are bonded onto one surface of a clear elastic rectangular beam. Then the beam is bent either by using a three-point load method or by clamping one end and deflecting the other. Assuming a

perfect bonding of the fibers to the beam, the strain in the fiber at any point would be equal to the strain at the surface of the beam at the same location. Kink band formation, which is a compressive failure mode of polymeric fibers under compression, is observed in-situ under the optical microscope by holding the beam in the bend position. The last kink band along the fiber, called the critical kink band, is recorded to calculate the strain at this point. This strain is called the critical compressive strain of the fiber, and used to calculate compressive strength of the fiber by multiplying it by the tensile elastic modulus of fiber, or in case of Kevlar™ fibers, by fiber compressive modulus from composite data, assuming that the fiber is linear elastic. (See the Section 3.2)

Elastica Loop Test

Elastica loop test was first performed for glass fibers by Sinclair [3] to measure their tensile strength. Later, Jones et al. [4] used it to determine the intrinsic strength and non-Hookean behavior of carbon fibers. Allen [6] conducted the elastica loop test to observe the compressive behaviors of PBZT and PPTA fibers.

Basically, a loop in a fiber is twisted and the loop size is reduced by pulling on the loop ends until the first kink band is observed at the bottom of the loop where the critical bending stresses are developed. As mentioned before, kink band formation in the compression side of the

fiber is assumed to occur just before elastic instability of fiber material. At this stage, the loop size is recorded from photographs. The radius of curvature can be calculated either from equations of elastica or from radius of the circle drawn into the loop. (See the Section 3.1.4.)

Embedding the Fibers in the Matrix

This test is conducted by embedding the fiber or the bundle of fibers in the matrix-especially epoxy-and by compressing it parallel to the fiber axis. This technique has been used to study compressive behavior of many fibers including carbon fibers, PBZT, and Kevlar™ fibers [18,11,19,20,16]. Compressed fibers are examined by optical microscopy to observe deformation modes in the fiber. Keller [16] reported that the matrix induced residual stresses on the fiber during the sample fabrication. This might cause some problems in measuring compressive properties of the fibers. Also the alignment of the sample during compression was another problem.

Recoil Test

As reported in [21], this technique is based on the fact that recoil forces act on the broken ends of fiber after tensile failure, causing damage to the fibers. This damage is the result of compressive stresses developed by snap-back, or recoil, whose magnitude exceeds the compressive strength of the fiber. The magnitude of the

compressive stress generated during snap-back or recoil is directly related to the magnitude of the tensile stress at failure. In this analysis, the recoil compressive strength is taken as the stress above which compressive damage is observed. It was reported that results from this test are in excellent agreement with compressive strengths measured in the composite tests for polymeric fibers.

Composite Compression Testing

As mentioned before, composite compressive testing is not feasible in the developing programs of fibers because the limited number of sample fibers are produced in laboratories. Also, to measure the composite compressive strength properties is difficult because the slight specimen geometric variations result in eccentricity of the applied load. This fact causes a geometric instability. Thus, in order to achieve an accurate measure of the compressive strength of a composite material, complex loading fixtures and specimen configurations are needed.

CHAPTER III

3. EXPERIMENTAL SET-UPS AND PROCEDURES

Introduction

As explained in Chapter I, two methods were usedto determine the compressive behaviors of the fibers: Elastica loop test and bending beam test. These two techniques will be explained in detail in this section, which includes their procedures, instrumentation used, advantages and disadvantages of the methods.

3.1. Elastica Loop Test

Generally, a loop in a fiber was twisted and the size of the loop was reduced gradually by pulling on the loop ends. At the same time, the fiber deformation was observed by optical microscope. Also the scanning electron microscopy (SEM) was used to observe the consecutive loops of the same fiber.

The elastica loop test was performed in two groups:

1. Optical microscopy method
2. Scanning electron microscopy method

The following three sections will explain the methods in detail.

3.1.1 Optical Microscopy Method

For Small Size Loops

The test was conducted on an optical microscope by inducing a loop in a fiber and trapping it in oil between a cover slip and a microscope slide. The loop size was reduced by pulling on the loop ends until the first kink band was observed at the bottom of the loop. Photomicrographs of kink bands and loops were taken at various stages as the test proceeded.

A fixture was designed for small size loops -especially for Kevlar™ fibers- to facilitate reducing the loop size. The top view of this fixture is given in figures 2(a) and 2(b). The overall set-up for this experiment is given in figure 3. The friction must be minimum between the surfaces. Since the fiber is so delicate, even a dust particle may be an obstacle to the loop. Therefore, light oil is used to overcome these difficulties.

Special care must be taken in applying in-plane forces at the end of loops. An acceptable gap between the two arms of the loop at the cross over point must be maintained. For this purpose, the loop is trapped between two glasses with an interval of about 100 μm. Also, it was observed that oil helps in keeping the two arms together.

Tension is applied on both ends of the loop in the same direction by using fixture knobs. (See Figure 2(a) and 2(b)).

Loop size measurements have been done by using

Figure 2(a). Fixture Used for Elastica Loop Test

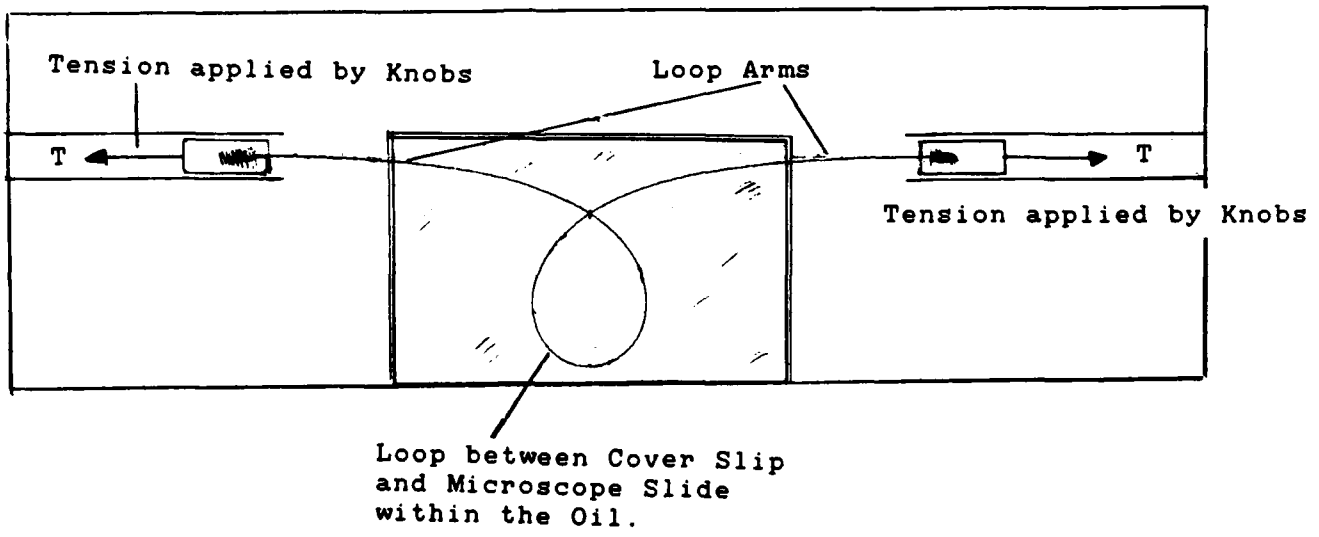

Figure 2(b). Schematic of Fixture for Elastica Loop Test

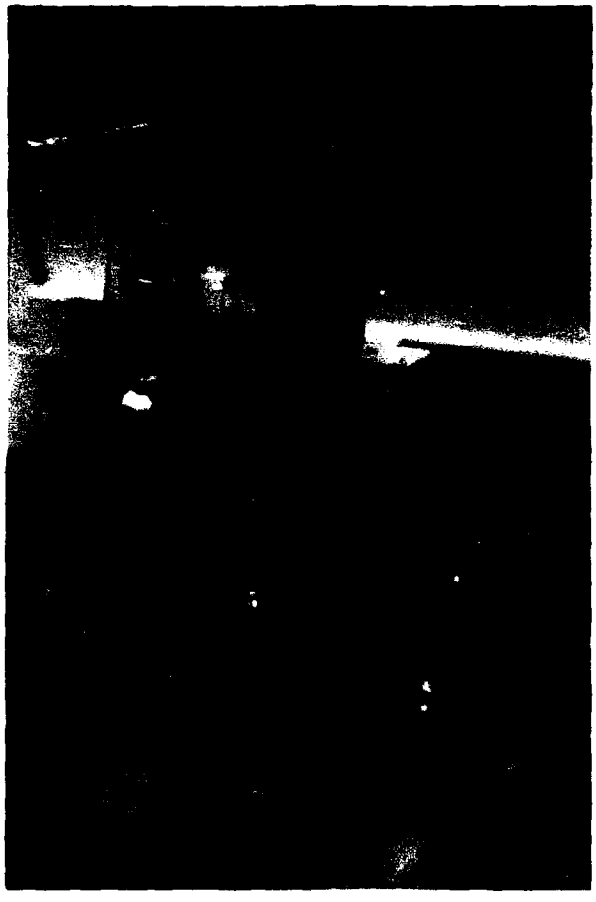

Figure 3. Overall Set-Up for Elastica Loop Test

photomicrographs taken at various stages of the loop, while its size is being reduced. (For various stage definition,see Section 4.4). To calculate the critical strain in the fiber, the photographs of the loop stages at which the first kink bands were observed was used. The minimum radius of curvature, thus the strain in the fiber, was calculated by using two methods: One assumes that the loop is formed from the infinite elastic bar. Its mathematically defined shape, known as the elastica, is given in [3]. The other uses the radius of a circle drawn into loop. (See Section 3.1.4)

For Large Size Loops

This method was used for Heat Treated PBZT, As Spun PBZT and Heat Treated PBO fibers. Since the loop sizes were large, the fixture explained above was no longer used to reduce the loop sizes. But, the same procedure and the same precautions, were observed as in the previous section. Instead of a fixture, a glass plate was used to hold the loop.

Instead of trapping the loop between cover slips, it was kept in a plane by tensioning a fiber over it with a certain distance from the loop. Also oil is used to have smooth movements of the loop.

The direct measurement of loop geometry at various stages has been made by using a grid placed below the glass plate. Stereo Zoom microscope was used to read the exact

dimensions of the loop. Only elastica formulation method (See Section 3.1.4.) was used to calculate the minimum radius of curvature and subsequently the compressive strain at the compression side of the fiber.

3.1.2 Scanning Electron Microscopy (SEM) Method

This method was conducted to observe very small fiber surface deformations, which could not be detected by optical microscope. The following procedure was applied: The different sizes of loops were twisted in a fiber and were placed on the SEM specimen holder. The size of each loop was very close to the one in which the first kink bands were observed by optical microscope. No oil was used while reducing the loop size, because later, the fibers were needed to be coated for SEM. The loops were kept in place by tensioning one or two fibers over them. (See Figure 21).

The fibers were coated with Au/Pd (10 nm layer) in Balzers Mini Deposition System (MED010) to minimize charging in the electron beam. This system is shown in figure 4.

SEM observations were carried out by using JOEL scanning electron microscope (Figure 5) at 20 KV. It was pointed out [6] that the degradation due to radiation is not a problem for Kevlars™ and PBZT fibers under the above observation conditions.

The kink bands at the bottom of the loop were observed first. Then, one arm of the loop was traced until the last detectable kink band on the surface of the fiber was found.

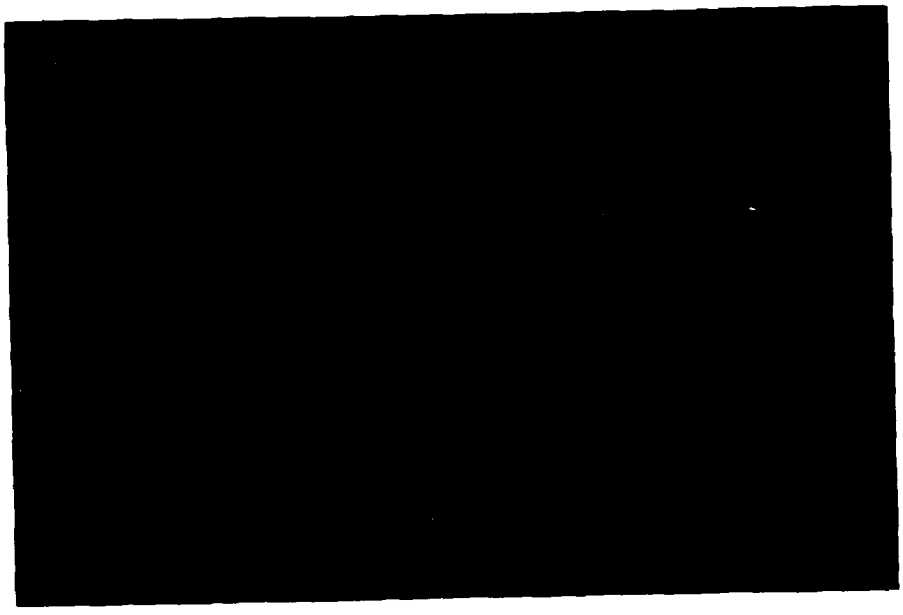

Figure 4. Mini Deposition System (MED010-Balzers)

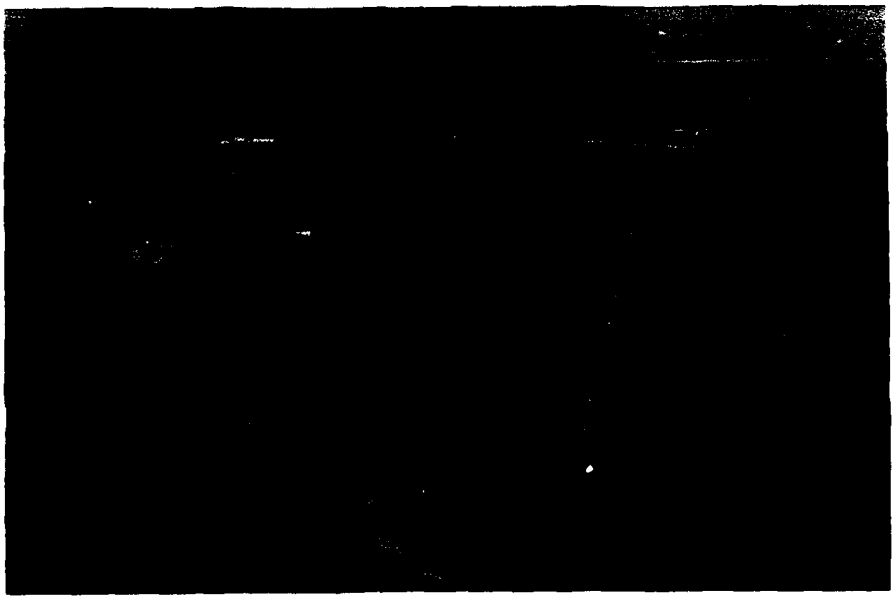

Figure 5. Scanning Electron Microscope (SEM)

Photomicrographs of critical kink band and the loop were taken for calculation of compressive strain at that location, where the last kink band was seen. Minimum radius of curvature was derived from the circle radius, drawn in the loop at the same location. Critical compressive strain in the fiber was calculated by:

$$e_{cr} = \frac{r}{R_m}$$

where e_{cr} = critical compressive strain

r = fiber radius

R_m = minimum radius of curvature of the location where the last kink band is seen.

3.1.3. Advantages and Disadvantages of Elastica Loop Test

Advantages:

1. Simple in nature.
2. Easy to take measurements.
3. Surface irregularities are not a problem, because the compressive deformation is observed on the compressed side of the fiber.
4. In-situ observation of the fiber deformation may give more information about fiber compressive behavior.

Disadvantages:

1. Special care must be taken to apply the in-plane forces.

3.1.4. Theoretical Consideration of Elastica Loop

The elastica loop test for single filament fibers was first used by Sinclair [3]. He measured the tensile strength and Young's modulus of glass fibers. Later, this test was used by some additional workers [6, 4, 7] to measure either tensile or compressive properties of single fibers.

Basically, Figure 6 shows the geometry of the elastica loop. A moment balance about any point p (x,y) gives:

$$M = M_T + T\,(S-y) \tag{1}$$

where M_T is bending moment at the end of loop arm and

T is tension applied to the fiber ends.

The radius of curvature can be written as:

$$\frac{1}{R_m} = \frac{d^2y / dx^2}{[1+(dy/dx)^2]^{3/2}} \tag{2}$$

and the normal bending moment equation:

$$M = \frac{E\,I}{R_m} \tag{3}$$

Neglecting M_T and by substituting the equation (1) into (2) and (3), one obtains:

$$\frac{1}{R_m} = \pm \frac{p\,dp/dy}{(1+p^2)^{1/2}} = b\,(S-y) \tag{4}$$

where $p = dy/dx$

$b = T / EI$. The positive sign applies where R_m is positive and the negative sign applies where R_m is negative.

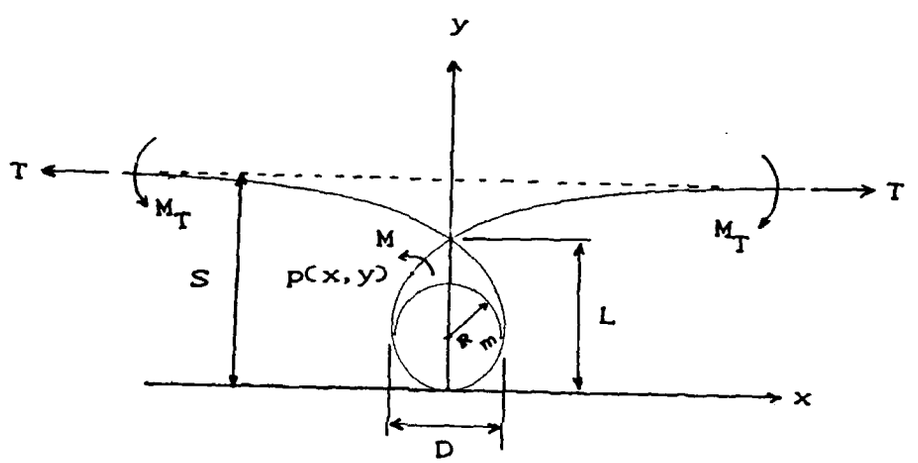

Figure 6. Geometry of Elastica Loop

Integrating equation (4) gives:

$$\pm 1/(1+p^2)^{1/2} = 1/2\ b\ y^2 - b\ S\ y + c \qquad (5)$$

To evaluate the constants b and c :

At y = 0, dy/dx = p = 0. Therefore, using positive sign, c = 0.

At y = S, dy/dx = p = 0. Therefore, using negative sign, $b = 4/S^2$

So equation (5) becomes:

$$\pm 1/(1+p^2)^{1/2} = (2y^2/S^2) - (4y/S) + 1 \qquad (6)$$

Integrating equation (6) gives:

$$x = \pm\ S \left[\frac{2y}{S} - \frac{y^2}{S^2}\right]^{1/2} \mp \frac{S}{4} \operatorname{Ln} \left[\frac{1+(2y/S - y^2/S^2)^{1/2}}{1-(2y/S - y^2/S^2)^{1/2}}\right] \qquad (7)$$

This analysis yields very important results:

$$S^2 = \frac{4\ E\ I}{T} \qquad (8)$$

$$D = 0.5328\ S \qquad (9)$$

$$L = 0.7136\ S \qquad (10)$$

$$R_m = S/4 \qquad (11)$$

where S is the distance from the arm to the bottom of the loop.

D is the minor axis of the loop.

L is the major axis of the loop.

R_m is the minimum radius of curvature.

E is elastic modulus.

I is moment of inertia.

(See Figure 6 for the above terms.)

Note that for an elastic fiber in the elastica loop

test, the ratio of major to minor axis would be a constant,

$$L/D = 1.34 \tag{12}$$

This ratio will be used for checking the fiber deviation from elastic behavior in chapter IV. The ratio of major to minor axis (L/D) against major axis (L) will be plotted for each fiber to show the compressive behavior of the fiber drawn into the loop in Section 4.4.

Allen [6] studied any possible curvature contributions due to shear and material anisotropy. He concluded that the curvature contribution due to shear and material anisotropy is negligible and equation (3) can be used to describe the elastica loop for anisotropic fibers.

Another important point in this study is that, the onset of kink band formation due to compressive stresses precludes the attainment of a tensile failure in the loop which is more commonly observed for brittle materials [6]. Note that if there is a material imperfection in the tension side of the fiber, it is possible to have tensile failure in the loop before a kink formation.

The radius of curvature at the onset of kink band formation can be calculated by using two methods. One uses the equation [11] and dimensions of the loops at the onset of kink band formation. For large loop sizes, a grid placed below the loop is used to measure the loop dimensions. In the second method, the calculation of radius of curvature is carried out by measuring the radius of a circle drawn into the loop as shown in figure 6. Note that Figure 6 has been

plotted by using equation [7]. Also the circle inside the loop has been drawn theoretically, so that minimum radius of curvature at the bottom of the loop are equal for both geometries.

After calculating the minimum radius of curvature, the compressive strain in the fiber can be calculated by:

$$e = \frac{r}{R_m}$$

where r: fiber radius

R_m: minimum radius of curvature.

The comparison of the critical strains obtained from the methods explained above will be given in chapter IV.

3.2 Bending Beam Test

In this technique, fibers are bonded on clear elastic rectangular beam. The beam with the fiber is bent and fiber deformation is observed in-situ with an optical microscope. It is assumed that the fiber is perfectly bonded to the beam, and thus strain at any point in the fiber will be equal to the strain at the surface of the beam at the same location. (See Figure 7)

3.2.1. Preparation of the Samples.

A single fiber was mounted under a certain tension onto the surface of a clear plexiglass, parallel to the length of the beam (6 mm x 25.7 mm x 152 mm). Tension is calculated for each fiber to give them a tensile prestrain of 0.03%.

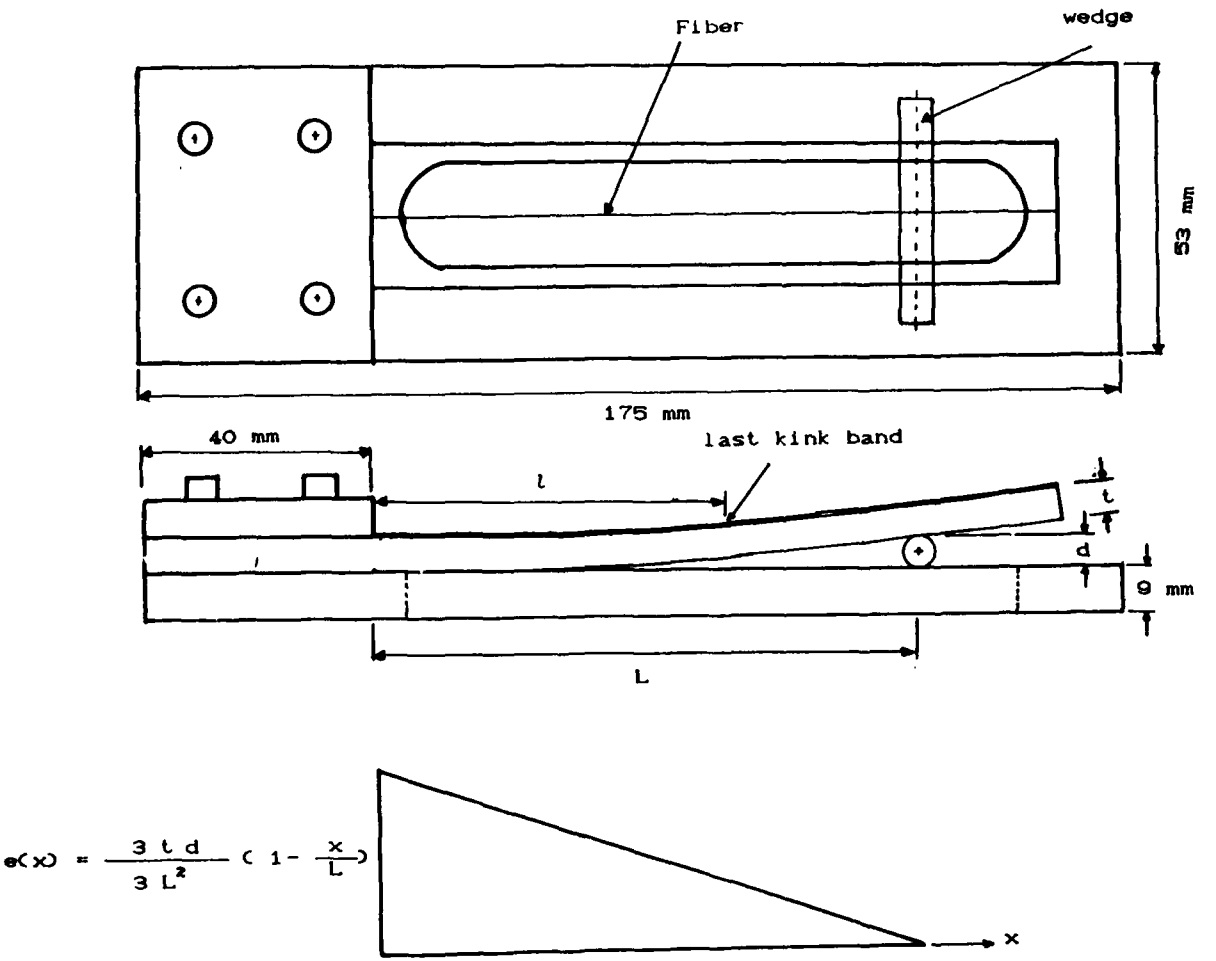

Figure 7. Schematic Drawing of Bending Beam Test Apparatus and Strain Distribution in the fiber

Several layers of urethane coating (MS470) were sprayed over the beam (Figure 8). It was allowed at least 24 hours for the coating to dry completely. Also, a fast drying coating was chosen in order to prevent any humidity effect of the coating onto the fiber.

Since the coating is so thin relative to the beam thickness, no shrinkage of coating film was expected. Therefore, any residual compressive stresses on the bonded fibers is prevented. To make sure, each fiber was examined with optical microscope for any possible fiber deformation due to the bonding and handling before each test was conducted.

3.2.2. Procedures of Bending Beam Test.

The following procedures and precautions were observed during the bending beam test:

1. Before the test, all bonded fibers were examined by optical microscope for any deformation due to the coating and handling.

2. The beam was clamped in the fixture as shown in figure 9.

3. The fixture was mounted on the traveling stages as shown in figure 10. Note that the stage scale is parallel to fiber and is convenient to measure the horizontal distances from any point along the fiber to the clamped edge.

4. The experimental set-up for bending beam test is shown in figure 11. For the equipment list, see the

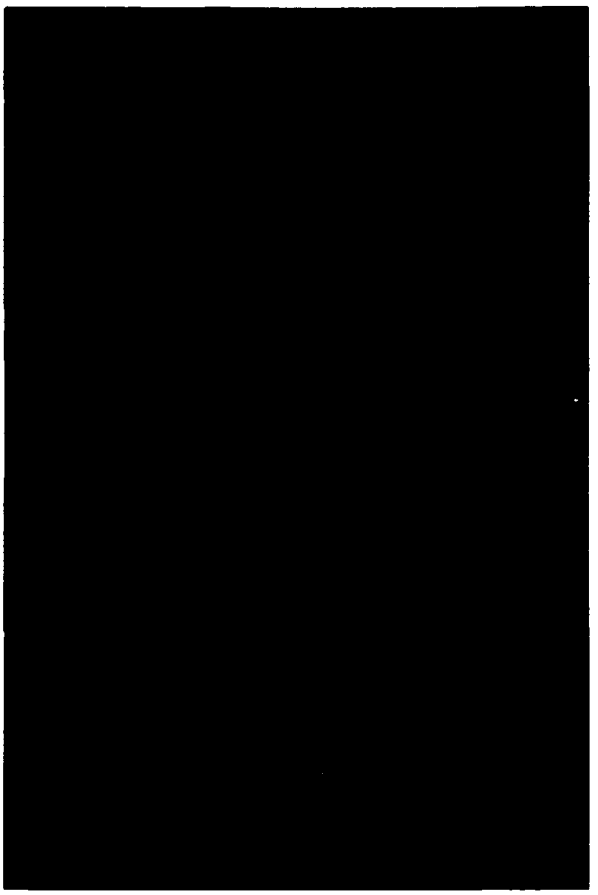

Figure 8. Specimen Preparation for Beam Test

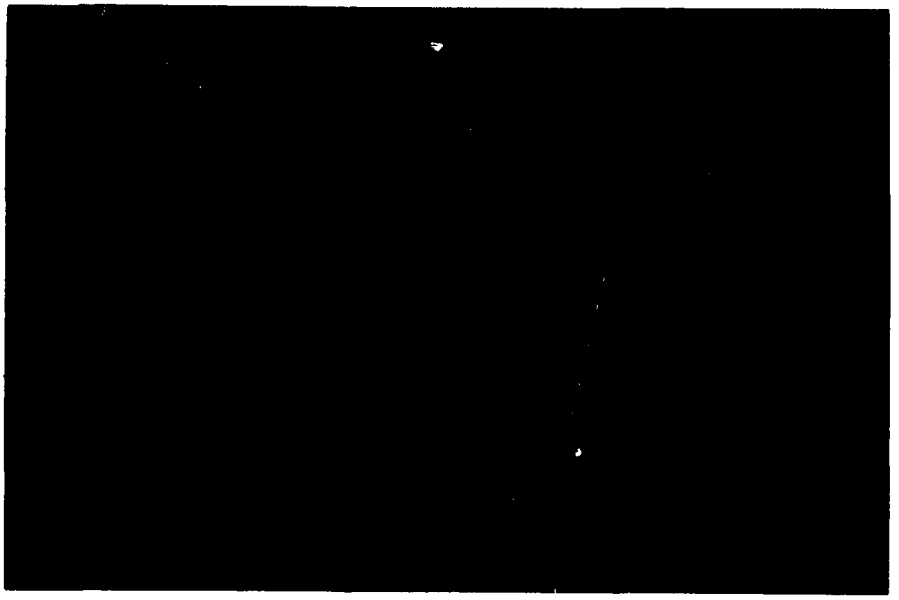

Figure 9. Beam with Bonded Fiber Clamped in the Fixture

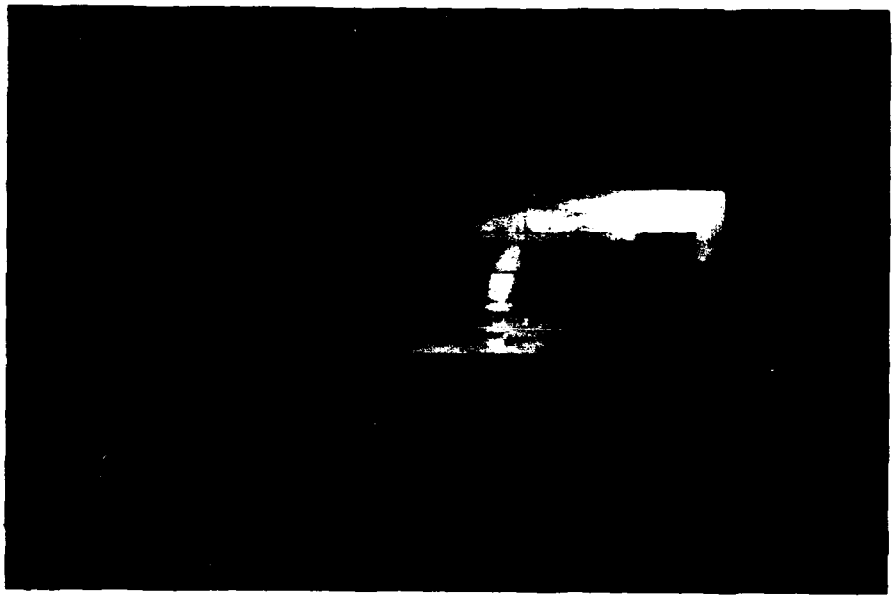

Figure 10. Travelling Stage with Fixture and Beam

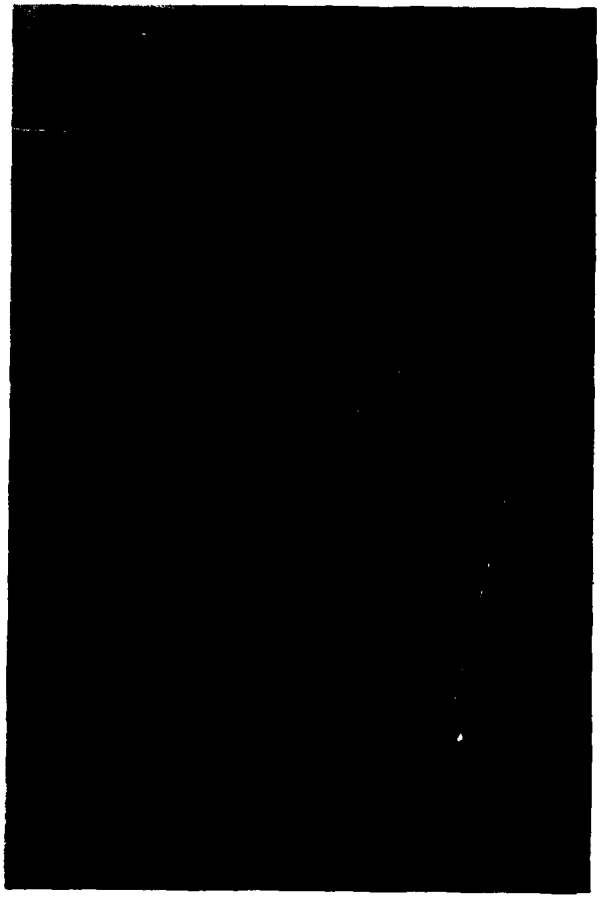

Figure 11. Experimental Set-up for Bending Beam Test

appendix-A.

5. A circular wedge was inserted between the beam and the base plate of the fixture to deflect the beam. It was possible to obtain many data points from one beam by changing the wedge or by moving the wedge closer to the clamped end of the beam. (See figures 12 and 13)

Since the surface of the beam was milled, it was hard enough to resist any deformation due to the contact of the wedge. Also a slight shift at the contact point of the wedge with the beam from the top of the wedge is neglected. (See Figure 7). Therefore the diameter of the wedge was accepted as the deflection of the beam.

6. It is felt that the deflecting rate of the beam is very important in terms of strain growth rate in fiber. Hence, loading the beam was performed slowly to make sure that coating and fiber combination on the beam surface is less affected.

7. Fibers were examined in-situ with optical microscope by holding the beam in the bent position. The distance L from the clamped end of the beam to the wedge center, and distance l from the clamped end to the point where the last kink band was seen along the fiber were measured by using stage scale (See Figures 12,13). The compressive strain at any point in the fiber at a distance of x from clamped end is assumed to be equal to that at the surface of the beam at the same location. By using linear beam theory,

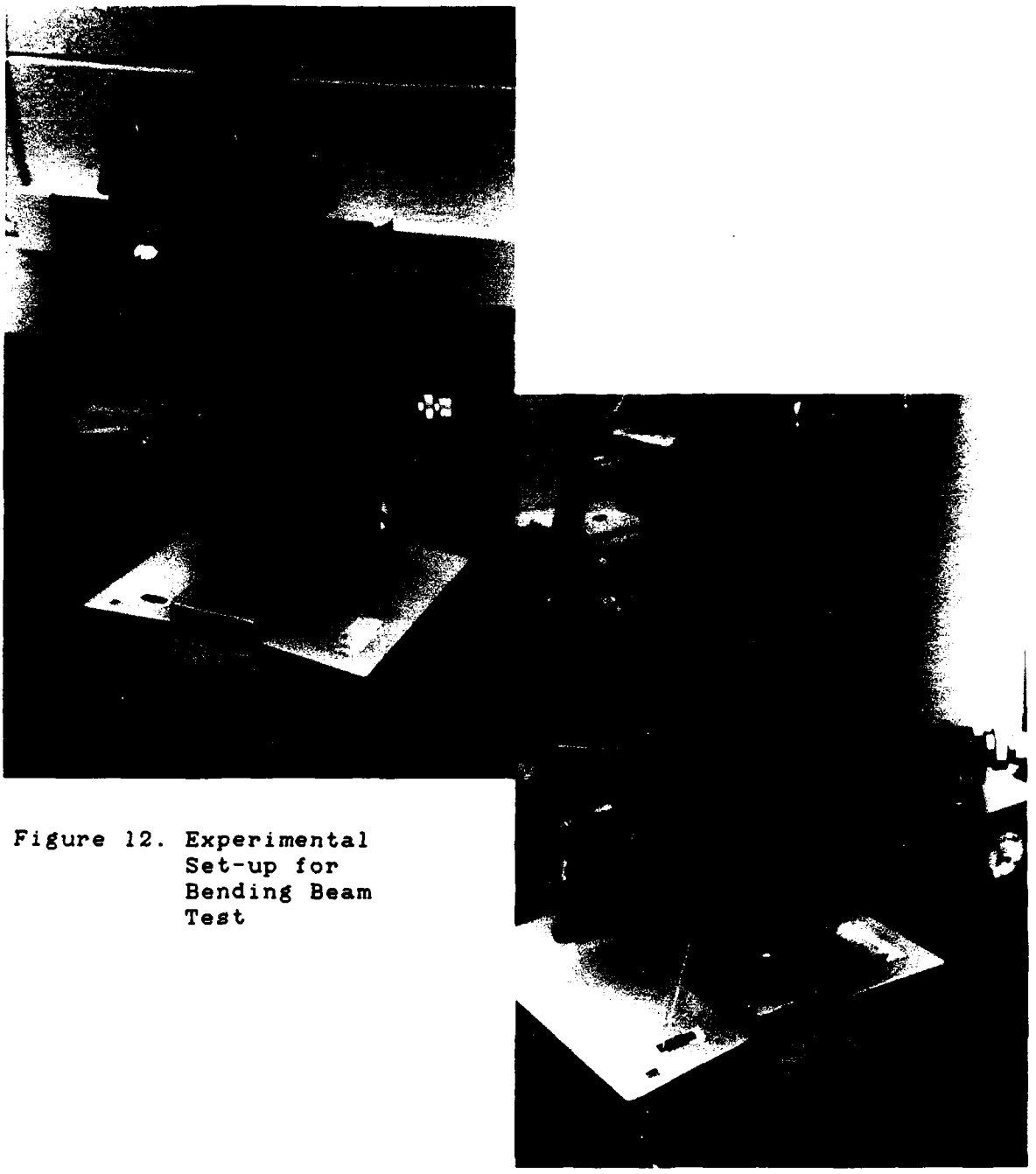

Figure 12. Experimental Set-up for Bending Beam Test

Figure 13. Experimental Set-up for Bending Beam Test

$$e(x) = \frac{3\ t\ d}{3\ L^2}\ (\ 1 - \frac{x}{L})$$

where t: thickness of the beam

d: wedge diameter or deflection of the beam

x: the distance from clamped edge to the location where the strain is calculated

L: the distance from the clamped edge of the beam to the wedge center

Note that this equation holds for the small curvatures of the beam. (See Figure 7)

The critical compressive strain of the fiber was found by replacing the distance l, from the clamped edge to the last kink band observed, in place of x in the equation above. The fiber axial compressive strength was calculated by multiplying the critical compressive strain by the fiber axial tensile modulus, or fiber compressive modulus obtained from the composite data, assuming that the fiber is linear elastic until the critical kink band is formed.

3.2.3. Advantages and Disadvantages of Bending Beam Test

Advantages:

1. Simple test in nature.
2. Easy to take measurements.
3. In-situ observation of fiber deformation, while loading the beam, is very useful in examining the fiber compressive behavior.

4. The axial stress gradient created along the fiber is very advantageous in observing the fiber compressive behavior at different stress levels. This axial stress gradient can be changed easily by varying the wedge size or by moving the wedge close to clamped end.

5. It was reported [16] that, in matrix-fiber combination, matrix shrinkage is a problem in testing fiber compressive properties. Bending beam test eliminates this drawback by applying a very thin coating relative to the beam thickness.

Disadvantages:

1. Some fiber surface imperfections make it impossible to observe critical kink bands in the fiber by optical microscope. For instance, AS PBZT had such surface irregularities so that it was not possible to distinguish the critical kink bands with surface imperfections. (See Section 4.4.5.)

2. Kink band formation in Kevlar™149 and T-300 fibers could not be observed even if the beam was defected beyond small deflection concept. This indicates that these two fibers take large compressive strains for failure.

CHAPTER IV

4. Results and Discussion

4.1 Introduction

Bending beam and elastica loop tests were performed for seven polymeric and three graphite fibers. The next section gives the overall test results. Also, the results are discussed and compared with the results available in the literature. Then, a new approach to kink band formation is discussed in Section 4.2. The compressive behavior of each fiber is discussed separately in later sections. In the last section, a comparison of the results of the two methods will be made.

4.2. Overall Results and Discussion

Overall compressive test results obtained from this study are given in table I. The values were calculated by using the test procedures explained in Chapter III. Table II gives some results obtained in previous studies. The comparisons between them should be made with great caution because of different techniques used. Also the fiber conditions such as heat treated or not, may affect the results.

Generally, compressive strengths of fibers obtained from bending beam and elastica loop tests are slightly

Table I. Critical Strains and Compressive Strengths of Fibers, obtained in this study.

FIBER	DIA (mm)	E (GPa) [1]	ELASTICA LOOP TEST ecr(%) Optical Micros. radius	ELASTICA LOOP TEST ecr(%) Optical Micros. elastica	ELASTICA LOOP TEST ecr(%) SEM radius	BEAM TEST ecr(%) [2]	COMPRESSIVE SRENGTH, σc (GPa) Beam Test [4]	COMPRESSIVE SRENGTH, σc (GPa) Elastica Loop [4,5]
KEVLAR 29	0.012	78.6	.75 ∓.12	.69 ∓.02		.75 ∓.10	.59	.50
KEVLAR 49	0.013	110.3	.81 ∓.12	.61 ∓.05		.69 ∓.04	.69	.67
KEVLAR 149	0.013	119.8	1.65 ∓0.12	1.09 ∓0.09		- [3]	-	1.24
HT PBO [6]	0.080	152.0		.91 ∓.02		.18 ∓.03	.27	.47
HT PBO [7]	0.065	166.0		.26 ∓.02		.19 ∓.01	.32	.43
HT PBZT	0.017	303.0		.13 ∓.01	.11 ∓.02	.10 ∓.05	.30	.39
AS PBZT	0.020	110.0		.15 ∓.01	.13 ∓.01	- [8]	-	.17
T-50	0.007	393.0				1.04 ∓0.08	4.09	-
P-75S	0.010	517.0				.52 ∓.07	2.69	-

1 Composite compressive modulus for Kevlar fibers; Tensile modulus for the rest of the fibers
2 Corrected for tensile prestrain applied during mounting to beam.
3 Not able to see kink band formation.
4 Calculated by $\sigma c = E \times ecr$
5 Calculated by using ecr in fifth column.
6 Treated by 5 % NH_4OH
7 Steam 1 type
} Produced in Materials Laboratory.
8 Not able to get this value because of fiber surface irregularities.
∓ values are standard deviations.

Table II. Compressive Strengths of Several Fibers obtained by Previous Workers in different test methods.

FIBER	COMPOSITE σ_c (GPa) [15]	BEAM σ_c (GPa) [15]	LOOP [15] σ_c (GPa)	RECOIL [21] σ_c (GPa)	EMBEDDED IN RESIN [18] σ_c (GPa)
KEVLAR 29	.40, .47	-	-	.97	.49
KEVLAR 49	.99, .48	.74	.74, .79	.95	.85
KEVLAR149	.92, .45	-	-	-	-
PBO	.20	.28	.68	.20	-
PBZT	.26, .41	.45, .52	.68	.27	.28, .42
T-50	1.61	-	-	-	-

* Note that compressive strength values depend on several factors; for detail, refer to references.

higher than those obtained from the composite compression test (Column two in table II.). This is very normal and expected. It is believed that the most important effect on these differences is the availability of the controls on the test parameters. It is obvious that composite compression test parameters are less controllable than single filament test parameters. For example, let's take the matrix and fiber interaction during fabrication of composite samples. Keller [16] reported that the sample fabrication using epoxy matrix caused critical compressive failures in the polymer fibers. The shrinkage of the matrix material during fabrication resulted in residual compressive stresses in the fiber so that some kink bands had been observed. A similar situation may occur during composite fabrication. Consequently the residual compressive stresses might lower the value of compressive strength obtained from composite compression test.

There is one exception in the above discussion; the compressive strength of HT PBZT. It is very comparable to the composite compressive strength.

The table II is given for overall comparison of the compression test methods for reader's convenience. The results for each fiber, obtained in this study will be discussed separately in the Section 4.4.

4.3 Kink Band Consideration

Modeling Kink Band Formation

Careful observations with optical microscope on the kink bands during the bending beam test showed that, the so called kink bands are made of many fine black lines grouped together with a certain angle to the fiber axis. First of all, let's depict it in Figure 14, based on the pictures of kink bands in Figures: 22 to 30.

In Figure 14 (a), one observes the typical critical kink band observed in the bending beam test. (See Figure 30 (a)). For the sake of our discussion, only plane A-A with angle α to the fiber axes (α is kink band angle) will be considered. A similar collection of fine black (cloudy) lines parallel to the plane A-A may progress in the direction parallel to the planes B-B and C-C, as the strain increases. This critical kink band is nothing but accumulation of many faint (cloudy) black lines parallel to the plane A-A. It is believed that each faint black line represents the buckling of separated microfibrils due to the elastic instability. These lines are totally recoverable if the load is released. It is most likely that they are on the region close to the surface of fiber.

If the compressive strain increases in the fiber, the core of the black line group gets darker and many faint (cloudy) black lines are added to the group, parallel to the

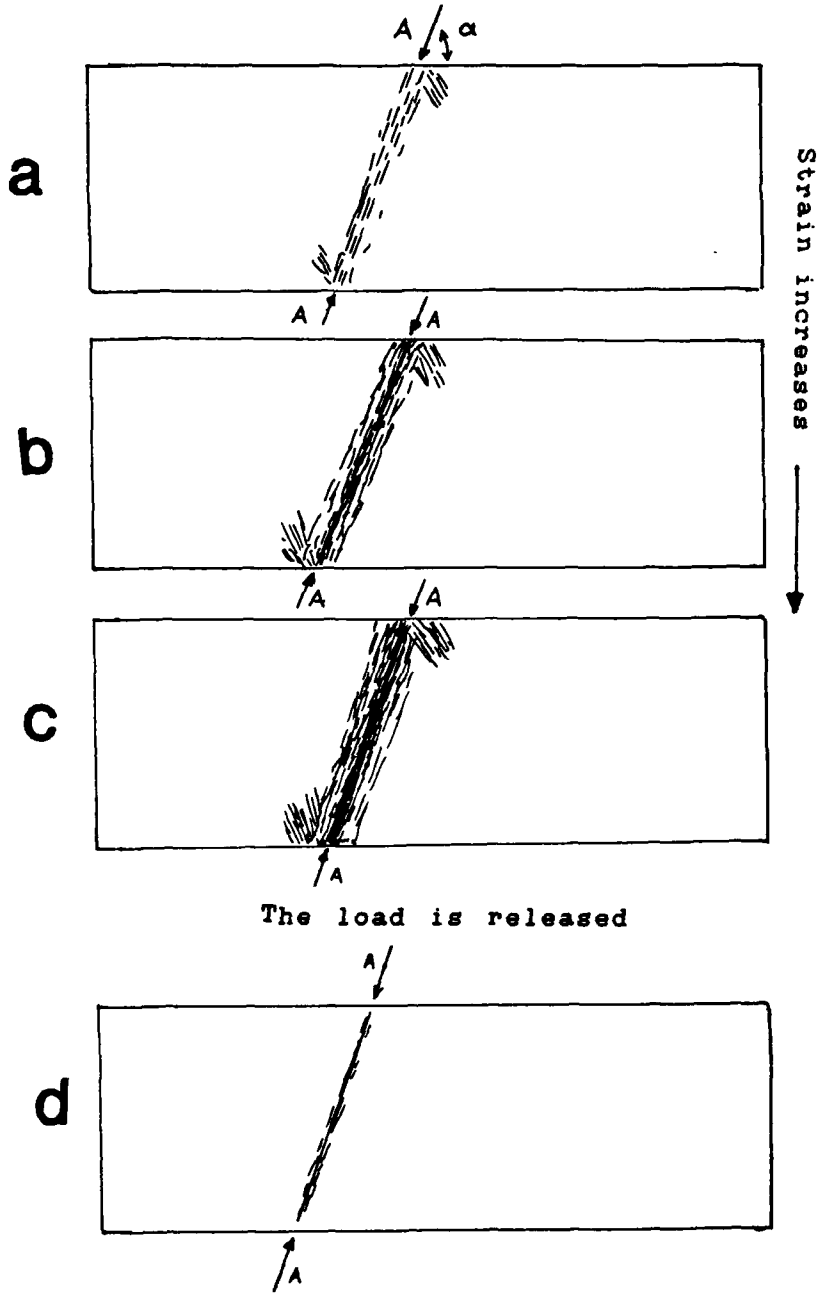

Figure 14. Kink Band Formation

plane A-A. This occurrence is depicted in Figure 14 (b) and (c). (Also see Figures 30,31,32). It is believed that getting the core darker means that the separated and buckled microfibrils are progressing through the fiber. If the load is released at stage (c), in Figure 14, the faint (cloudy) black lines are disappeared around the core but the shadow of core remains as pictured in Figure 14 (d). (See Figures 30(d), 31(d)).

We may draw some conclusions from the overall picture above: Each faint black line parallel to plane A-A represents the separated and buckled microfibrils, as seen by optical microscope. They are recoverable if the load is released. This conclusion is compatible with the elastic instability criteria for the critical kink band formation by DeTerasa [8].

Each faint black line parallel to plane A-A acts as a hinge, which results in compressive stress concentration in this plane when the compressive strain increases. Consequently, more black lines are seen around plane A-A as well as the core of these black lines get darker, which means that, buckling and separation of microfibrils are progressing through the fiber. At the same time, it is believed that some plastic deformation at the molecular level may occur in this core region. This molecular deformation may explain the permanent damage observed in the fiber after unloading. The molecular level plastic

deformation was studied by Keller [16] and Takahashi and others [19].

Helical Kink Band Observations

Helical kink band formation can be easily observed by looking at the pictures of kink bands in the fiber. For example, Figure 31(c) clearly shows a helical formation of kink bands around the fiber. Also, this fact was observed for all fibers by changing the depth of focus of the optical microscope. Figure 15 shows this kind of study for HT PBZT during the bending beam test. Helical compressive kink bands in cylindrically orthotropic materials such as wood and PPTA have been studied by DeTerasa [8]. He indicated that the PPTA fiber exhibits cylindrically orthotropic structural symmetry, like wood, formed by a collection of hypothetical radial sheets. A 'sheet' is the plane formed by the two mechanically strongest directions: longitudinal and radial. In the tangential direction, the strength and stiffness of materials are represented by relatively poor adhesion between those sheets. (See Figure 16). He concluded that the formation of kink bands in orthotropic materials result from shearing between the buckled plane of easy shear slip. This mechanism might be universal for orthotropic materials which are compressed parallel to the planes of easy shear slip. Helical kink bands in PPTA and wood result from the cylindrically orthotropic symmetry of these materials. Also he concluded that helical kink band

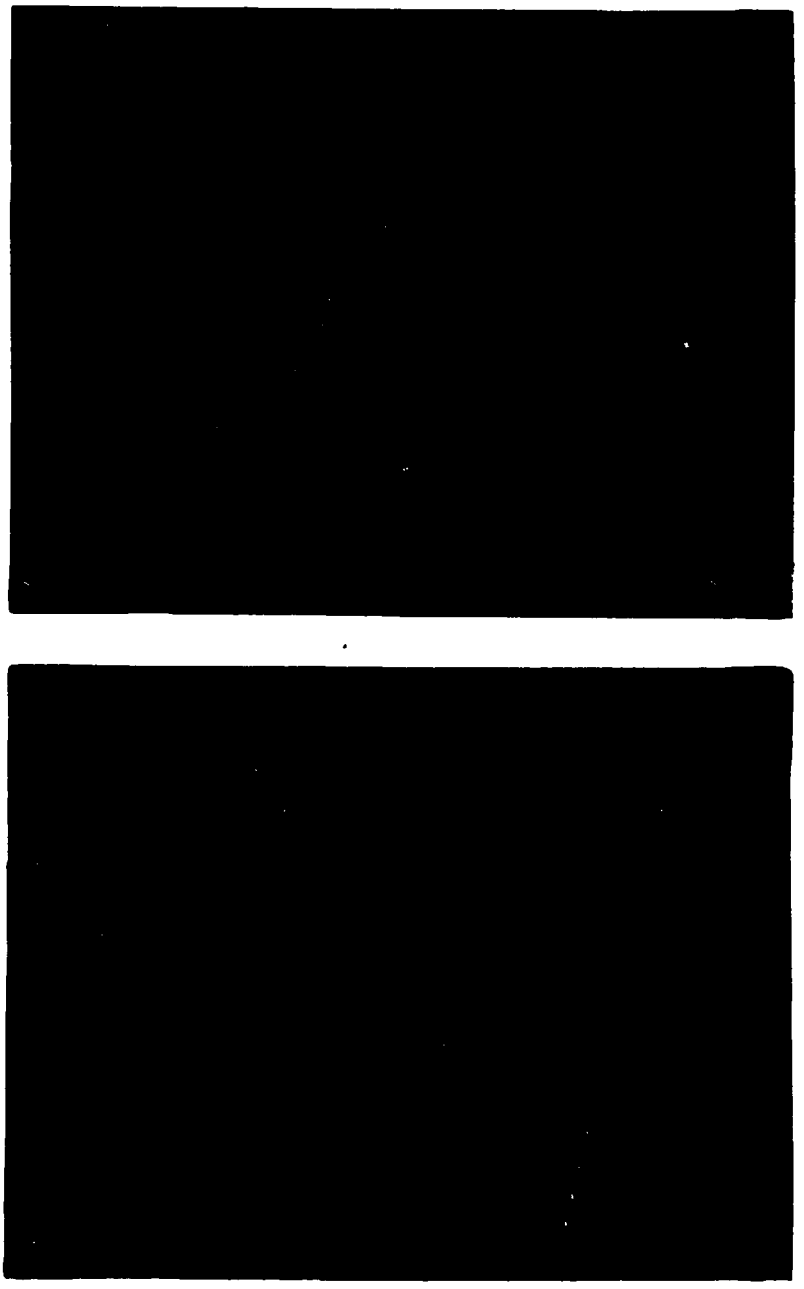

Figure 15. Helical Kink Band Observation in HT PBZT Fiber at Strain of .22 % (400X)

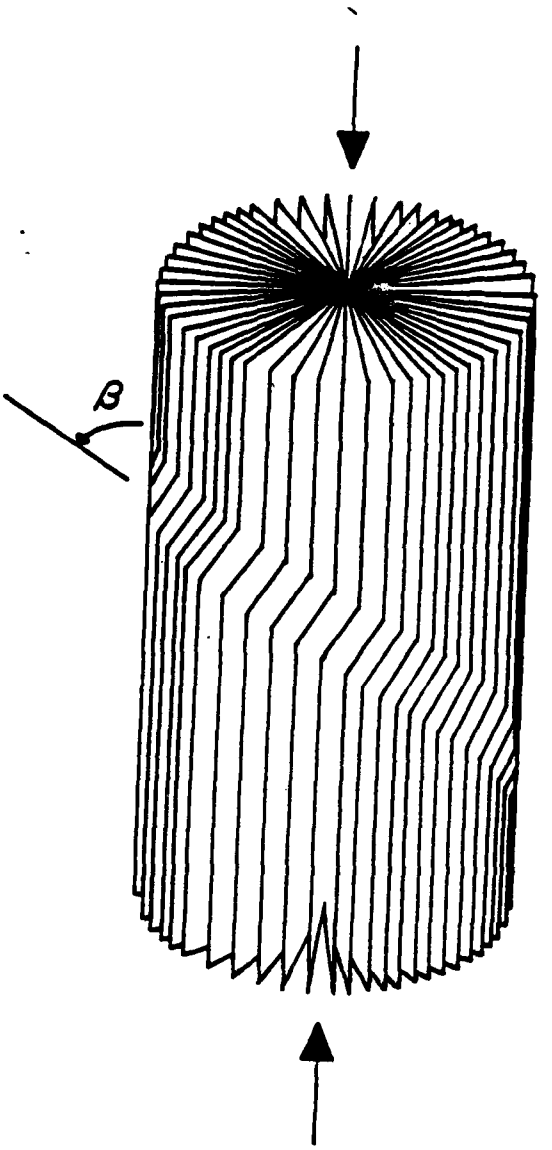

Figure 16. Illustration of Kink Band Formation in Cylindrically Orthotropic Material.(After [8]).

formation under axial compression should be exhibited by other cylindrically orthotropic materials which have the same mechanical anisotropy of wood and PPTA fibers. See Figure 16 for illustration of helical kink band formation.

Another concern is whether these helical kink bands are on the surface of the fiber or not. Does the internal deformation in the fiber along the kink band plane reach to the structural core of the fiber along radial direction? As we discussed in the previous section, kink bands initiate on the surface and propagate through the fiber cross-section as the strain increases. This fact can be realized easily by evaluating the kink bands under optical microscope. However, the extent of internal deformation due to the buckling of easy slip planes close to the fiber core could not be detected by optical microscopy. Also many workers [8,18] reported that kink bands were close to the surface of the fiber.

4.4 Compressive Behaviors of Fibers

In this section, compressive behaviors of Kevlar™ 29, Kevlar™ 49, Kevlar™ 149, HT PBO, HT PBZT, AS PBZT, T-50, T-300 and P-75S fibers will be reported as observed in the elastica loop and bending beam test. Comparisons with previous studies will be made in detail.

4.4.1. Compressive Behaviors of Kevlar™ 29 fibers

The Kevlar™ 29 fibers are a product of the Du Pont Company. Their compressive properties are given in the table III.

In this study, the compressive strain values of 0.63 - 0.75 % and 0.75 % have been obtained from the elastica loop and bending beam test respectively. To calculate the strength of Kevlar™ 29 fibers, the compressive strain values were multiplied by the fiber compressive modulus, calculated from unidirectional laminate compressive modulus. Also it is reported that the ratio of compressive modulus to tensile modulus is 0.8 - 0.9 for Kevlar™ 29 fibers [15]. So, the corresponding compressive strengths to above strain values have been found as 0.5 - 0.59 GPa and 0.59 GPa from elastica loop and bending beam test respectively. These strength values are close to composite compressive strength values of 0.393 -0.483 GPa. As explained in section 4.2, it is believed that the difference is resulted from the different test methodologies applied. Also the strength values obtained in this study are comparable to the strength

Table III. Compressive Properties of Kevlar™ 29

MODULUS (Fiber compressive modulus)*	E(GPa) [15]	78.6
STRENGTH		
→ Bending beam test	σ_c(GPa)	0.59
→ Elastica loop test	σ_c(GPa)	0.50 - 0.59
→ Composite [15]	σ_c(GPa)	0.39 - 0.48
CRITICAL STRAIN		
→ Bending beam test	ϵ_{cr}(%)	0.753 $\pm$ .098
→ Elastica loop test	e_{cr}(%)	0.634 $\pm$ .024 0.750 $\pm$ .120
→ Composite [15]	e_{cr}(%)	0.50 - 0.62

* Calculated from composite compressive data

of 0.43 Gpa obtained by L. T. Drzal [18]. He calculated the value from a compression test of embedding fiber in epoxy matrix. (See Section 2.4).

Wilfong et al. [1] stated that the critical compressive strain for seeing obvious kink bands is 2 % for Kevlar™29 fibers. They also indicated that this is surprisingly higher than the value of 0.8 % from its composites tress-strain curve. Since we found out the strain values of 0.63 - 0.75 % , which are comparable to the composite compressive strain value of 0.8 % ; the compressive strain value of 2 % for Kevlar™ 29 reported above can be invalidated. They also gave the critical strain compressive value for seeing obvious kink bands as 0.7 % for Kevlar™ 49, which is comparable to the values obtained in this study. (See Section 4.4.2).

Figure 17 gives the plot of the ratio of major to minor axis (L/D) against major axis (L) for the elastica loop test for Kevlar™ 29 fibers. Since the figure shows the behavior of the fiber under compression, it is important to interpret it in terms of compressive properties obtained from elastica loop test. Each data point in the figure was taken from measurements of the major axis (L) and minor axis (D) at any stage of the loops during the test. The plot is comparable to the one obtained in [5]. This means that the test has been performed properly. The (L/D) ratio remains constant ($\approx$1.34 ,solid line in the figure) until the major loop axis is of the order of 2.5 mm. Note that this

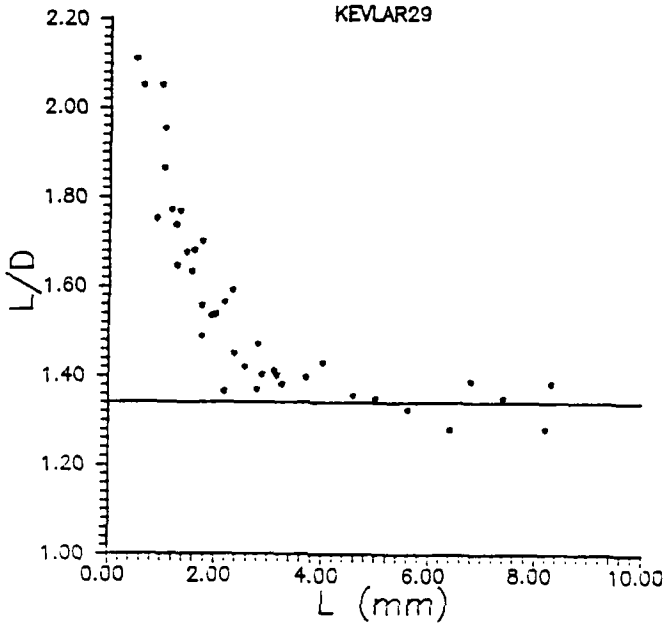

Figure 17. The Ratio of Major to Minor Axis (L/D) against the Major Axis (L) for Kevlar™ 29 Fibers.

constant line represents the elastic behavior of the fiber. (See the section 3.1.4). For smaller values of (L) (Less than 2.4 mm) the ratio (L/D) increases as the fiber deviates from elastic behavior. Also note that the bending strains are increased by decreasing the loop size (L).

The first kink bands at critical stage of the loop were observed at (L) values of 2.4 mm to 2.6 mm, which correspond to the (L/D) ratios of 1.37 to 1.56. Since the (L/D) ratios are higher than the constant value of 1.34, which shows that we are slightly above elastic line, the question arises about the validity of the results obtained from this study. Will this fact affect our results obtained from elastica loop test? Now let's consider above situation. The table IV gives (L) and (L/D) ratio data of the critical stages where the first kink bands were observed for different elastica loop tests. Also it gives the critical strains obtained from the elastica formulation and the radius of circle drawn into the loop as explained in the section 3.1.4. Note that when the (L) decreases from the test 1 to test 4 , the (L/D) ratio increases in the same order. This shows the deviation from elastic line (L/D = 1.34) according to elastica formulation. If the (L/D) ratio is 1.34 for a loop , the critical strain values obtained from two methods for the same loop are almost the same. This situation is explained in Section 3.1.4. in detail. For example if you consider the test 1 , the strain values obtained from two methods are almost the same

Table IV. Comparison of Critical Strains for Kevlar™ 29 Fibers, obtained from different Elastica Loop Tests.

Test No [1]	L (mm)	L/D	Elastica formula ε_{cr} (%) [2]	radius circle ε_{cr} (%) [2]	$\frac{\varepsilon_{cr\,elas}}{\varepsilon_{cr\,radi}}$
1	2.77	1.37	.60	.59	1.02
2	2.55	1.42	.63	.67	0.94
3	2.35	1.45	.63	.76	0.83
4	2.18	1.56	.66	.87	0.76

[1] Data taken from critical loop stages where the first kink bands are observed for each test

[2] Elastica formulation and radius of circle methods in calculating compressive strain in the fiber are explained in section 3.1.4

because we are very close to the (L/D) ratio of 1.34. Keeping in mind this fact , let's consider each method separately. The critical strain values obtained from elastica formulation for each test are given in the fourth column. If we take the strain value of 0.60 % for test 1 as a basis, the worst deviation (0.66 % of test 4) from this value is only 10 % while the deviation of (L/D) ratio from the elastic limit (L/D = 1.34) is 16 % . This shows that if one calculate the critical compressive strain by using elastica formulation and even if one has (L/D) ratio over the elastic (L/D) ratio, he will not get drastic changes in the final results. The fifth column of the table gives the critical compressive strains obtained from the radius of circle drawn into the loop. The similar consideration gives the 47 % deviation from the true strain value of 0.60 % while the (L/D) ratio deviation from 1.34 is 16 % . As a conclusion, the deviation slightly from elastic (L/D) ratio of 1.34 at critical loop stages in the elastica loop test does not change the final compressive strain values drastically. Generally, however the best strain values are obtained from the critical loop stage which has an (L/D) ratio of 1.34, in which both methods give the same strain values as in the test no.1.

Figure 18 (Part 1 and Part 2) give the photographs of typical loop stages of the same test taken while the size of the loop was being reduced. Note that picture (b1) shows the critical loop stage where the first kink bands were observed

in the fiber. The dimensions of this loop stage have been used to calculate the critical compressive strains in the fiber. The picture (b2) gives the first kink bands as observed in the optical microscope. The picture (a) shows the loop stage that no kink band was observed.

(a)

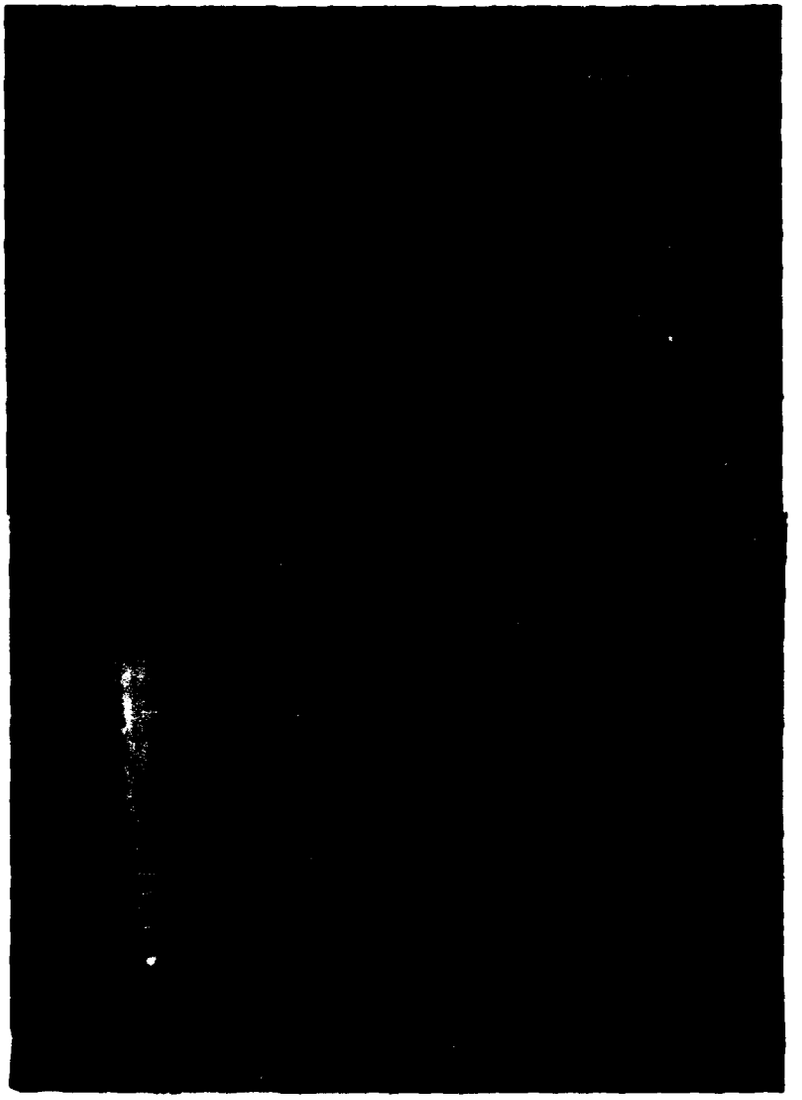

(b1)

(b2)

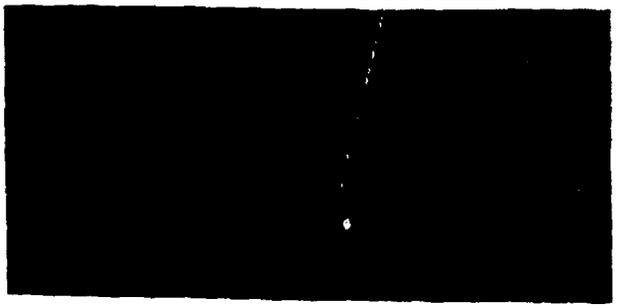

Figure 18. Reducing the Size of the Loop for Kevlar™ 29 Fibers *(Part 1)*

(d)

(e)

(f)

(g)

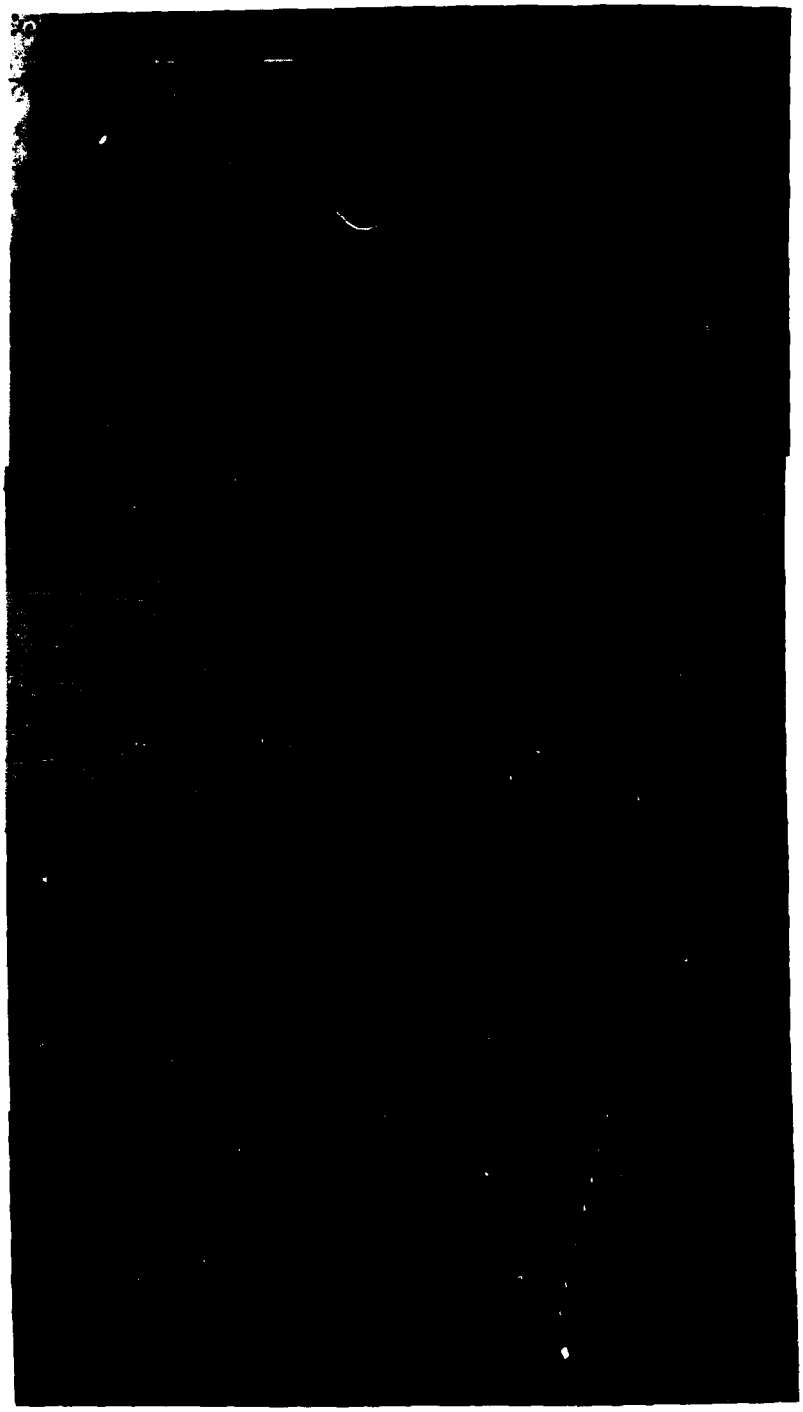

Figure 18. Reducing the Size of the Loop for Kevlar™ 29 Fibers (*Part 2*)

4.4.2. Compressive Behavior of Kevlar™ 49

Kevlar™ 49 fibers are a product of the DuPont Company which also has the Kevlar™ 29 and Kevlar™ 149 fiber series. It has a tensile strength of 3.5 GPa and a Young's modulus of 120 GPa. Its compressive properties are given in table V.

In this study, the compressive strength values for Kevlar™ 49 fibers of 0.69 GPa and 0.67 GPa were obtained from the bending beam and elastica loop test respectively. Note that the strength value of 0.76 GPa from the elastica loop test has been calculated by using elastica loop formulation as explained in Section 3.1.4. If we use the minimum radius obtained from a circle drawn into the loop (See Section 3.1.4.), we could get a compressive strength value of 0.89 GPa. This conservative value is expected because the curvature of the fiber is not circular and the true curvature at that point is smaller than the value obtained above. Comments on calculating minimum radius of curvature, thus compressive strain in the fiber, have been made in Section 4.4.1. The above results are comparable to those obtained from the same tests conducted by previous workers. (See table II).

The compressive strength for Kevlar™ 49 obtained from composite compressive test is about 0.4 GPa, which is about 67% of the above values. General comments have been made on the comparison of composite test results with bending beam

and elastic loop test results in the Section 4.2. Here, the results will be discussed in detail by taking into consideration Figure 19, which shows compressive stress strain-curve for Kevlar™ 49/epoxy unidirectional composite [1]. As we see in this figure, the yielding is initiated at a compressive strain of about 0.3%. An ultimate compressive failure stress in the composite of 28.2 Mpsi (0.26 GPa) is reached at an ultimate compressive strain of .6%. The ultimate stress was normalized to get compressive strength for Kevlar 49 fiber as 62-67 Mpsi (0.43 MPa). Let's keep in mind the conclusion of Greenwood and the others [2]: 'The low compressive strength of Kevlar 49 composites is due to compressive failure in the fibers themselves, and not due to the resin or to the interfacial bond.' Therefore we can conclude that the apparent composite compressive strains are equal to the strains in the individual fibers of composite [22].

As seen in table V, the critical strains, which are 0.65% and 0.61% - 0.81% obtained from the bending beam test and loop test respectively, are comparable to the composite ultimate strain, but not its yield strain. Recall that our initial assumption for these tests was that the fiber behaves linearly elastic until the first kink bands are seen. However, the above comparison shows that the results are slightly beyond the elastic limits. Again one must be very careful about these comparisons because very small compressive strains are involved in the experiments.

Table V. Compressive Properties of Kevlar™ 49

MODULUS (Fiber compressive modulus)* [15]	E(GPa)	110.3
STRENGTH		
→ Bending beam test	σ_c(GPa)	0.69
→ Elastica loop test	σ_c(GPa)	0.67 - 0.89
→ Composite [1]	σ_c(GPa)	0.39 - 0.48
CRITICAL STRAIN		
→ Bending beam test	e_{cr}(%)	0.630 ± .036
→ Elastica loop test	e_{cr}(%)	0.610 ± .049 0.810 ± .120
→ Composite [1]	e_{cr}(%)	0.60 ultimate 0.30 yield

* Calculated from composite compressive data.

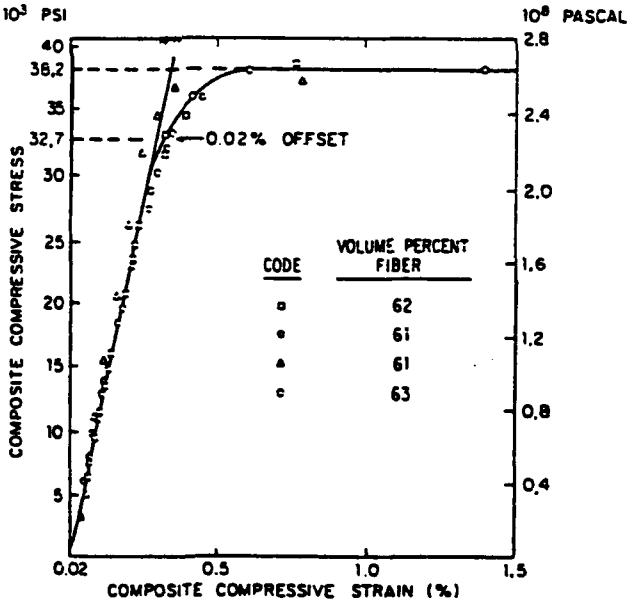

Figure 19. Compressive Stress-Strain Curve for Kevlar™ 49/epoxy Unidirectional Composite. [1]

Shall we look for the cause for this difference in experimentation methods or shall we look for a reason for being beyond the elastic limits in our tests? It seems that the deviation from elastic (L/D) ratio (L/D = 1.34) at critical stages may result in such a higher strength value for Kevlar™ 49. However, in Section 4.4.1., it is proved that the deviation from elastic (L/D) ratio (L/D = 1.34), doesn't cause a big impact on the results obtained from elastica formulation, but it changes the results obtained from the minimum radius of a circle drawn into the fiber.

Another comment on this issue can be made by approaching the problem in a different way. Recall, that the basis for these tests, done in this study, is the first kink band observations in the fibers. Let's change the basis for the elastica loop test and say that the loop dimensions at the stage just before the deviation from elastic (L/D) = 1.34 line (See Figure 20) will be used to calculate the critical strains in the fiber, even if no kink band will be observed at this stage. By taking into consideration the above criteria, the compressive strain in the fiber could be found as 0.45%, if the dimensions of the loop are taken as L=4.0 mm and S= L/ 0.7136 = 5.6 mm. (See Figure 20 and Section 3.1.4). This value is closer to the yield strain of composite test, but there is no theoretical basis for this assumption. The above assumption holds if one can prove that the fiber is deformed critically before the kink bands can be detected by all means.

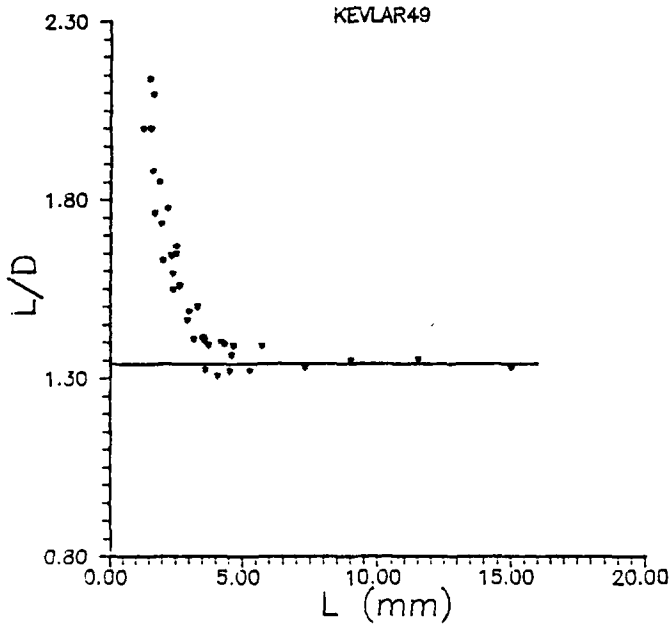

Figure 20. Ratio of Major to Minor axis (L/D) against Major Axis (L) for Kevlar™ 49 Fibers.

Figure 20 is comparable to the figures in the papers [2,5]. This shows that elastica loop tests have been done properly. Kink bands in the fiber and the loop shapes at two different stages can be seen in Figure 21: (a) shows critical stage, the first kink bands are observed at the bottom of the loop, (b) shows a later stage. Note how the kink bands grow and how the shape of the loop becomes progressively narrower.

The progressive growth of the kink band in the fiber with increase in compressive strain during bending beam test is shown in Figure 22. Please, refer to Section 4.3 for detailed explanation of kink band formation.

In Figure 23, some typical kink bands are shown at different strain levels. Note that after releasing the load, some shadows of kink bands could be seen as explained in Section 4.3.

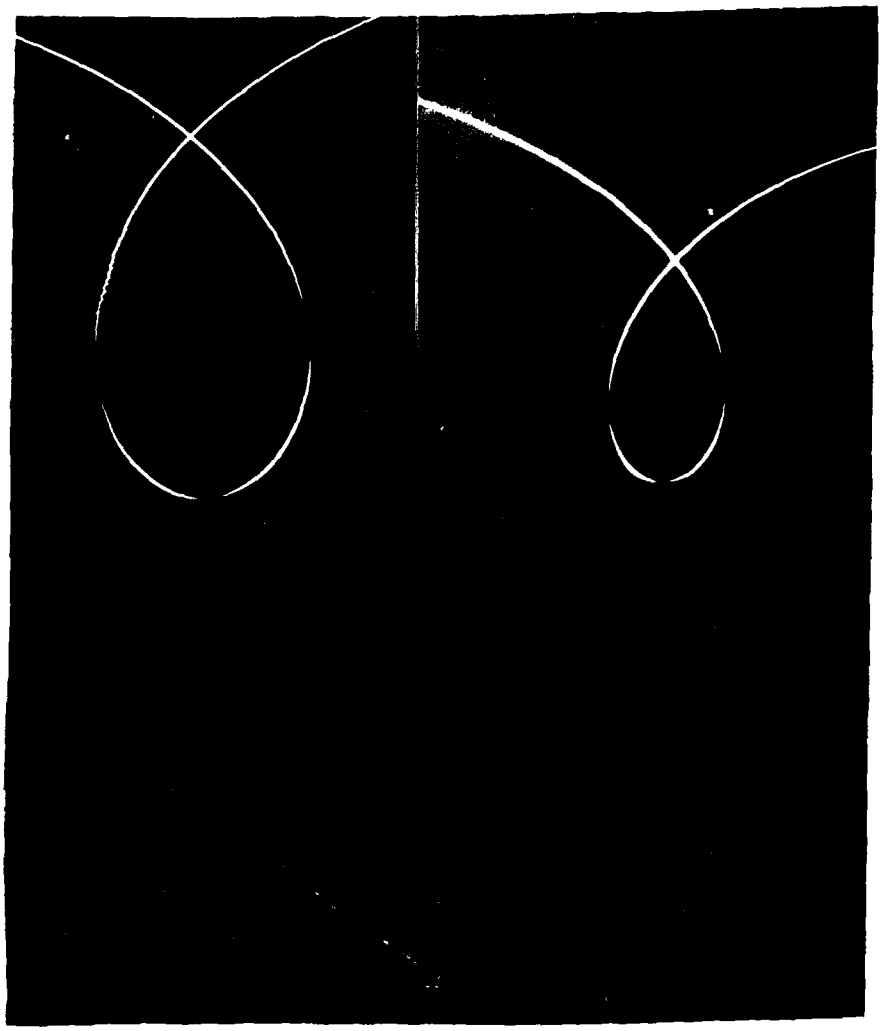

Figure 21. Kink bands in Kevlar™ 49 Fiber as observed by Optical Microscope at Different Loop Stages (a) shows the Kink Bands at Critical Stage. (b) Kink Bands at later Stage of the Loop (20X and 500X)

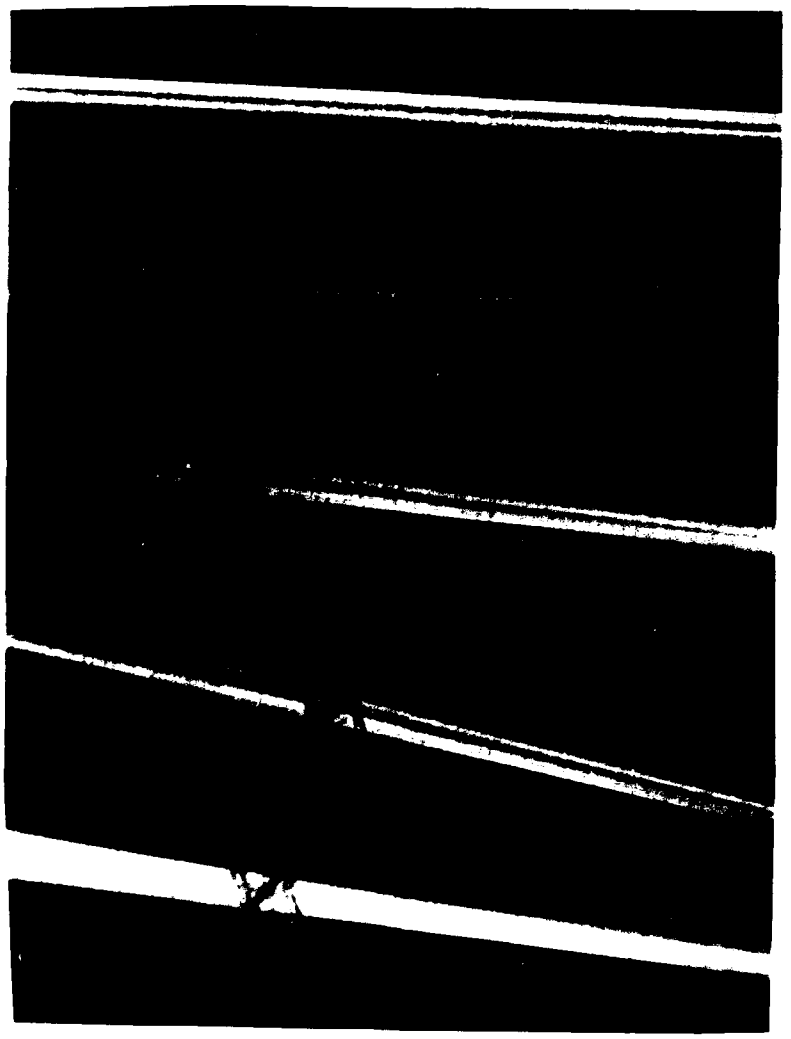

Figure 22. Progressive Growing of the same Kink Band with Increase in Compressve Strain in Bending Beam Test for Kevlar™ 49 Fibers. (500X)

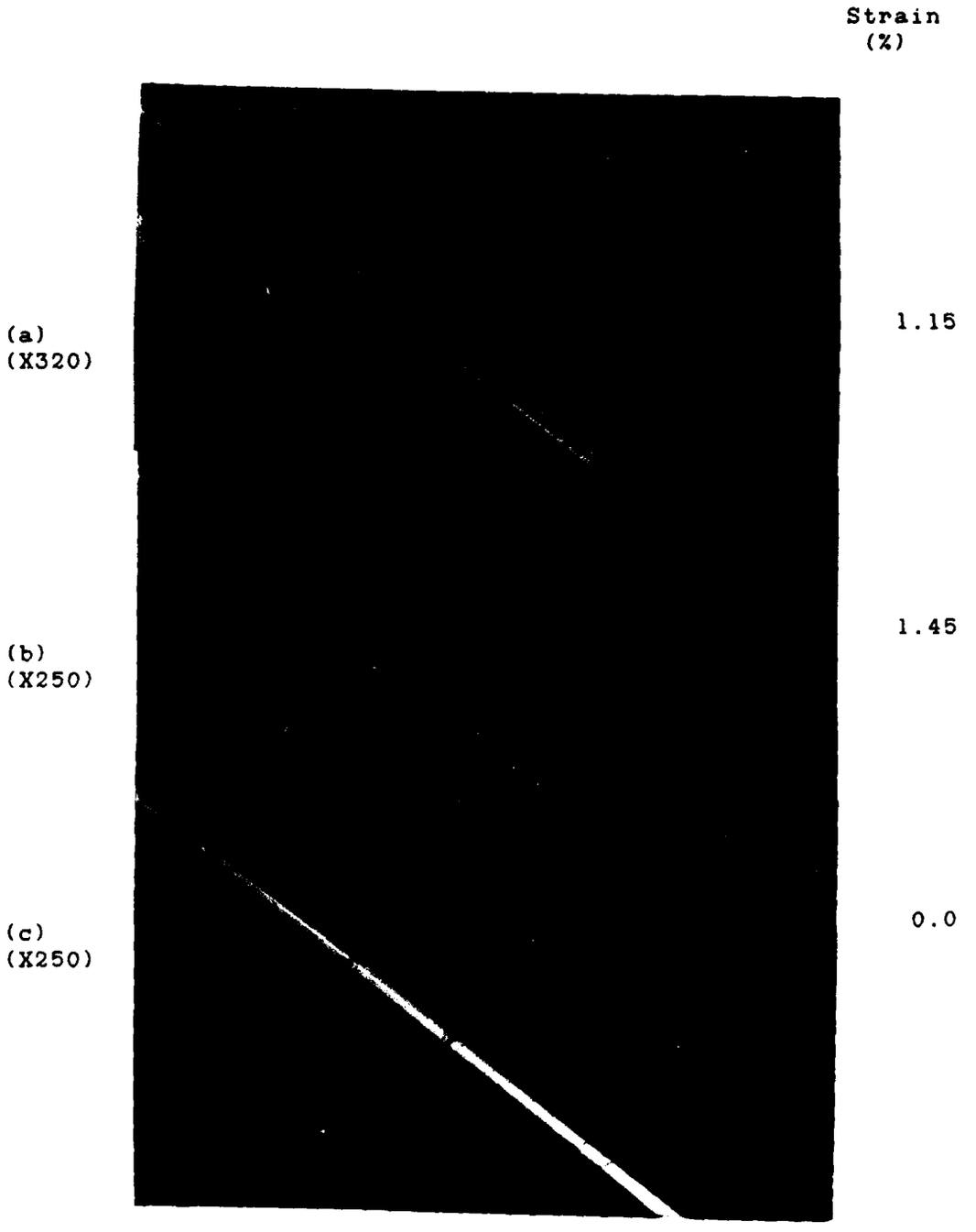

Figure 23. Kink Bands in Kevlar™ 49 Fiber during Bending Beam Test. (b) and (c) show the same location. (c) shows the Fiber after releasing the Load.

4.4.3 Compressive Behavior of Kevlar™ 149

Kevlar™ 149 fibers with a fiber compressive modulus calculated from composite data of 113.8 GPa are a product of Du Pont. They have a tensile strength and modulus of 3.45 GPa and 186.2 GPa respectively. The first time in the literature, the bending beam and elastica loop test were conducted for Kevlar™ 149. The results are shown in table VI.

Up to the limit of compressive strain obtainable in the bending beam test no kink bands in the fiber could be observed. This might be because of higher compressive strains required to deform the fiber. Just as, the elastica loop test showed that the fiber has a compressive strain of 1.09%. This value is higher than those obtained for Kevlar™ 29 and Kevlar™ 49.

Figure 24 shows the ratio of major to minor axis (L/D) against the major axis (L) plot. The data points are well above the elastic (L/D) ratio line (L/D = 1.34), up to the ratio of 1.60. It is observed that the tendency of the deviation from elastic L/D ratio increases with increase in compressive strength of the fiber. Recall that this deviation from elastic L/D ratio doesn't affect the critical compressive strain here drastically as explained in Section 4.4.1.

Figure 25 shows the progressive loop stages in the elastica loop test for Kevlar™ 149 fibers. Note how the loop becomes narrower. In Figure 26 (a), the first kink band can

be seen as observed by optical microscope. The Figure 26 (b) shows some kink bands just after the loop was crushed. The same location of the fiber after being stretched out is shown in this figure 26 (c). Note that the kink bands have disappeared.

Table VI. Compressive Properties of Kevlar™ 149

MODULUS (Fiber compressive modulus)*	E(GPa) [15]	113.8
STRENGTH		
→ Bending beam test	σ_c(GPa)	-
→ Elastica loop test	σ_c(GPa)	1.24 - 1.88
→ Composite [15]	σ_c(GPa)	0.32 - 0.45
CRITICAL STRAIN		
→ Bending beam test	e_{cr}(%)	-
→ Elastica loop test	e_{cr}(%)	1.090 ± .009 1.650 ± .120
→ Composite [1]	e_{cr}(%)	-

* Calculated from composite compressive data

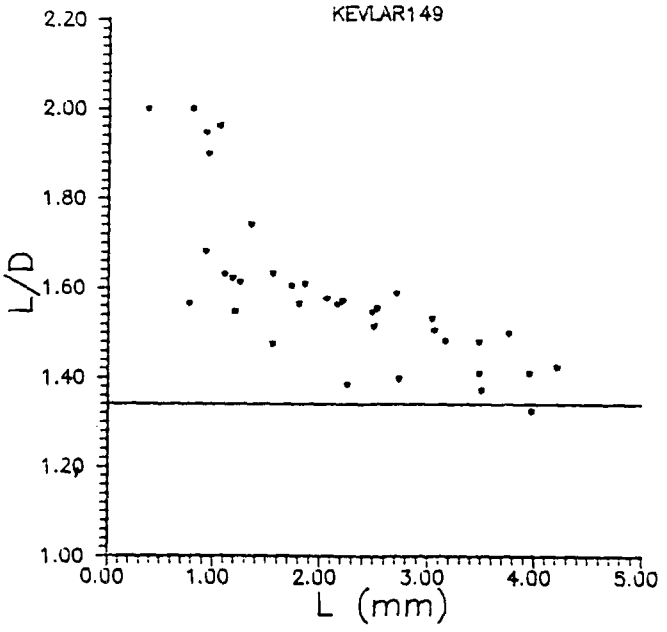

Figure 24 Ratio of Major to Minor Axis (L/D) against Major Axis (L) for Kevlar™ 149 Fibers.

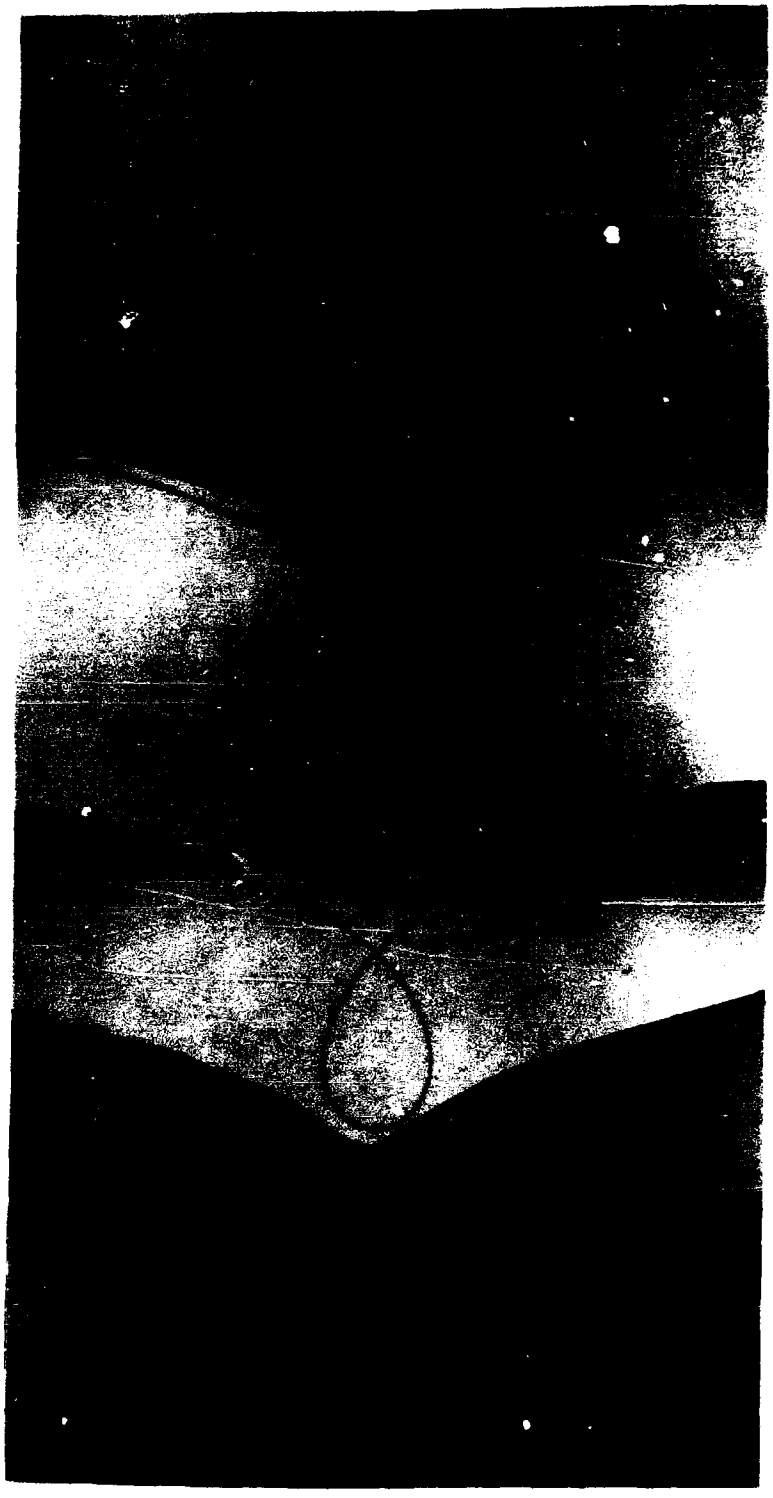

Figure 25. Progressive Loop Stages in the Elastica Loop Test for Kevlar™ 149 (X20)

Figure 26. (a) Kink Bands at the Bottom of the Loop in Kevlar™ 149
(b) Kink Bands just after the Loop was collapsed.
(c) The Same Place after stretching the Fiber out. (200X)

4.4.4. Compressive Behavior of PBO Fibers

PBO (poly (paraphenylene benzobisoxazole)), originally developed by Air Force Materials Laboratory, has tensile strength and modulus of 5.72 GPa and 358.5 GPa respectively. Also, higher property PBO fibers are available. The compressive properties of HT PBO (ST1) and HT PBO (NH_4OH) are given in table VII and table VIII respectively. Since these fibers were produced in Air Force Laboratories locally, the composite compressive strength of 0.20 GPa given in table II is not convenient for comparison [17-a]. Also the compressive strengths of these fibers obtained in this study cannot be compared with those obtained from the same tests given in table II, but generally, the values are of the same order.

The Figure 27 and 28 show the ratio of major axis to minor axis (L/D) against major axis (L) in elastica loop test for HT PBO (ST1) and HT PBO (5% NH_4OH) respectively. It is found out that the (L/D) ratio of the critical loop stages,in which the first kink bands were seen, is close to elastic (L/D) ratio of 1.34.

As seen in tables VII and VIII, the compressive strength values obtained from elastica loop test is slightly higher than those obtained from bending beam test. See Section 4.5 for explanation.

Figure 29 shows typical kink bands observed by optical microscopy at the bottom of the loop; (a) shows the critical

kink bands and (b) shows the kink bands at later stages. Figures 30,31,32 show typical kink bands at certain strains in the HT PBO(5% NH_4OH) fibers in bending beam test. Note how the kink bands are growing as explained in the section 4.3. The Figures 30 (d) and 31 (d) show the fiber after the load was released in the bending beam test. Note that while the shadow of the core of kink bands remains, the major portion of the kink band disappeared.

Table VII. Compressive Properties of HT PBO (ST1)

MODULUS (Tensile Modulus)	E(GPa)	165.0
STRENGTH		
→ Bending beam test	σ_c(GPa)	0.32
→ Elastica loop test	σ_c(GPa)	0.43
→ Composite	σ_c(GPa)	-
CRITICAL STRAIN		
→ Bending beam test	e_{cr}(%)	0.190 $\pm$ .010
→ Elastica loop test	e_{cr}(%)	0.260 $\pm$ .020
→ Composite	e_{cr}(%)	-

Table VIII. Compressive Properties of HT PBO (5% NH_4OH)

MODULUS (Tensile Modulus)	E(GPa)	151.7
STRENGTH		
→ Bending beam test	σ_c(GPa)	0.27
→ Elastica loop test	σ_c(GPa)	0.47
→ Composite	σ_c(GPa)	-
CRITICAL STRAIN		
→ Bending beam test	e_{cr}(%)	0.180 $\pm$ .030
→ Elastica loop test	e_{cr}(%)	0.310 $\pm$ .020
→ Composite	e_{cr}(%)	-

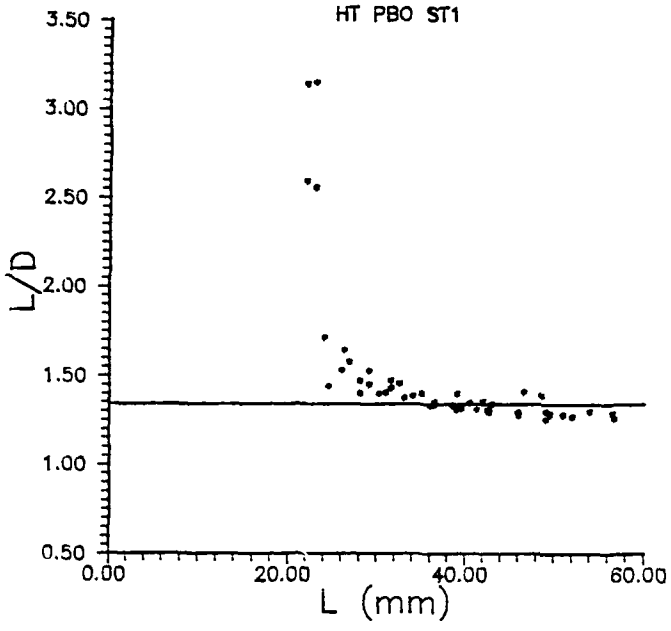

Figure 27. Ratio of Major to Minor Axis (L/D) against Major Axis (L) for HT PBO (ST 1)

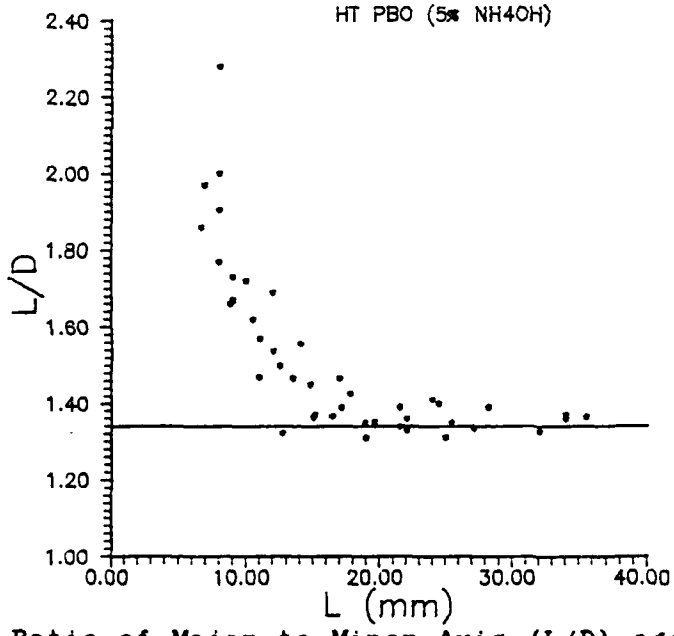

Figure 28. Ratio of Major to Minor Axis (L/D) against Major Axis (L) for HT PBO (5% NH4OH)

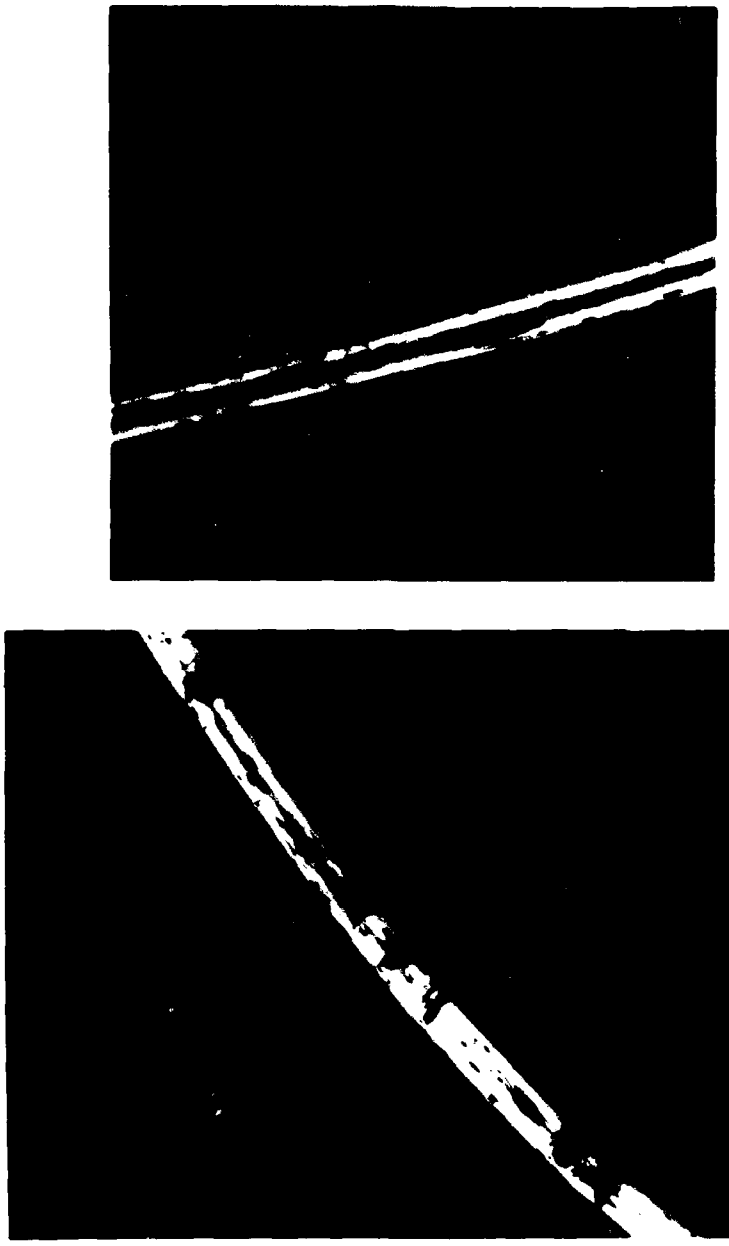

Figure 29. Kink Bands in HT PBO as observed by Optical Microscope during Elastica Loop Test.

(a)
Critical
Kinkband

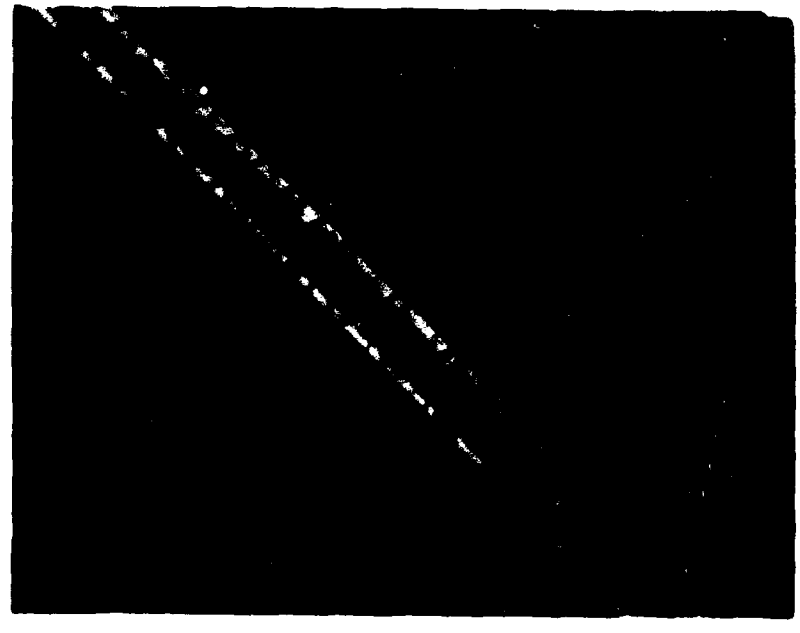

(b)

Figure 30 (a). Kink Bands in HT PBO (5% NH_4OH) observed by Optical Microscope during Bending Beam Test

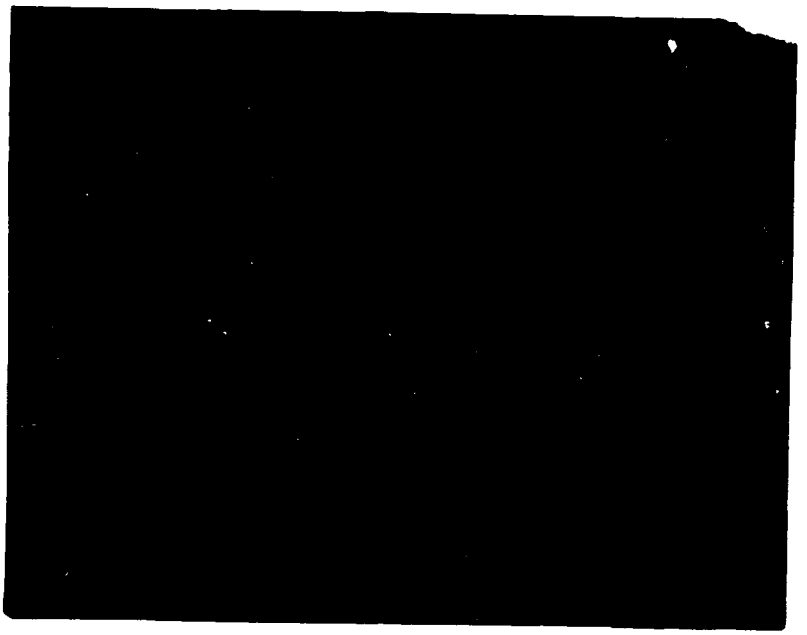

(c)

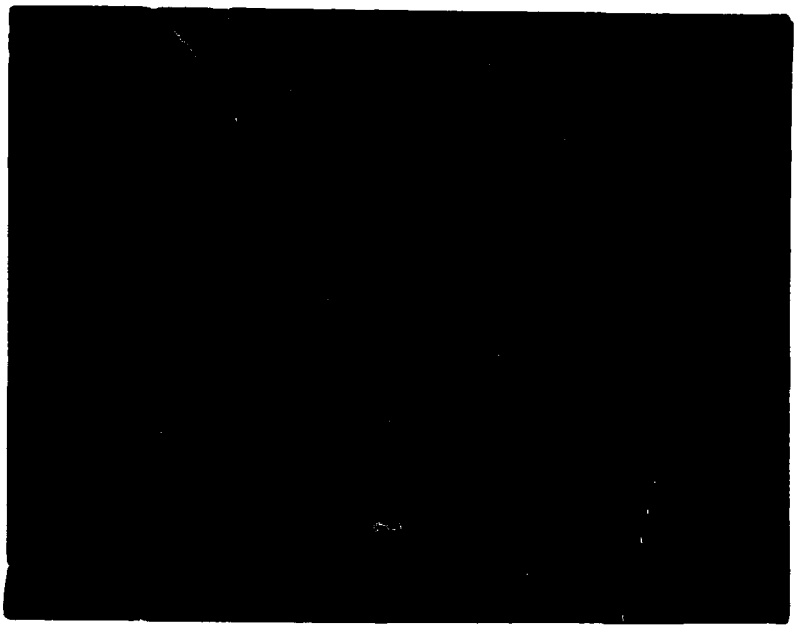

(d)

Figure 30 (b). Kink Bands in HT PBO (5% NH_4OH) observed by Optical Microscope during Bending Beam Test

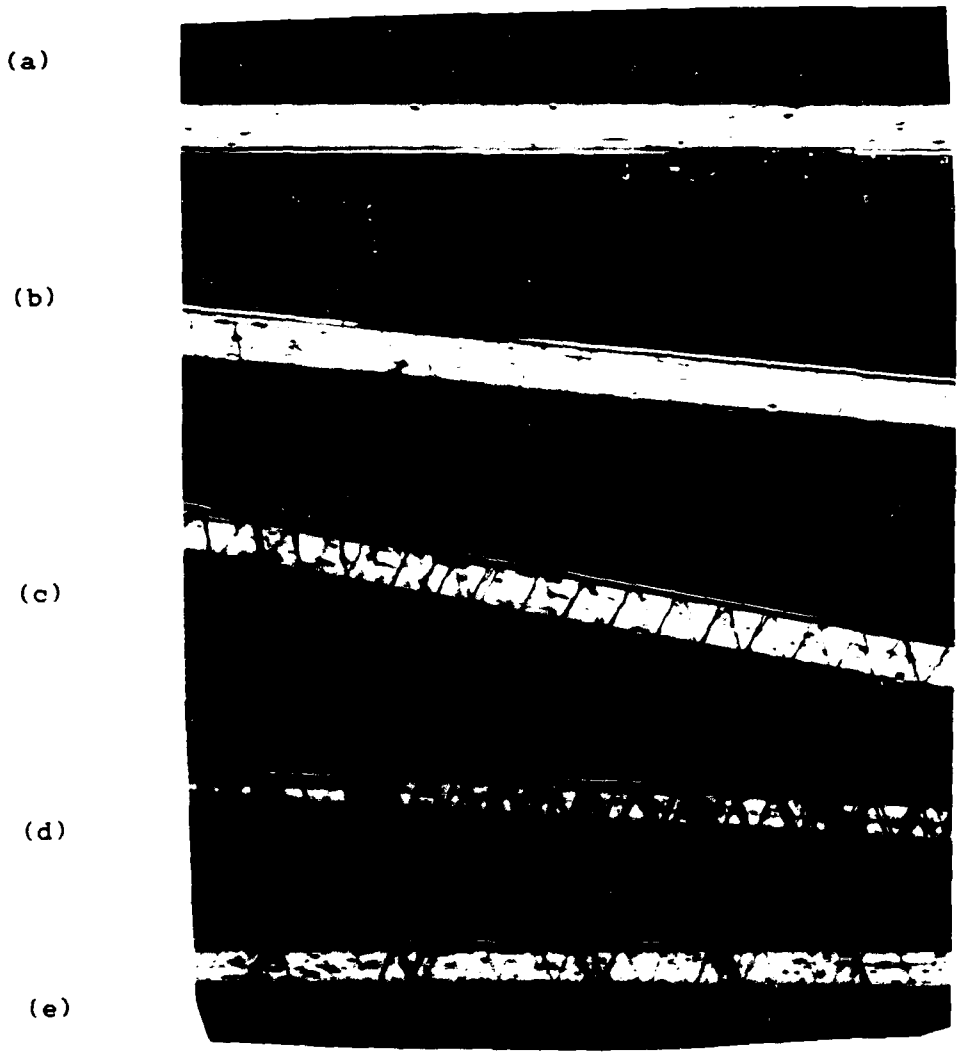

Figure 31. Kink Bands in HT PBO (5% NH_4OH) observed by Optical Microscope during Bending Beam Test

Figure 32 (a). Kink Bands in HT PBO (5% NH_4OH) observed by Optical Microscope during Bending Beam Test

(d)
e=.77%

(e)
e= 1.30%

Figure 32 (b). Kink Bands in HT PBO (5% NH_4OH) observed by Optical Microscope during Bending Beam Test

4.4.5 Compressive Behavior of PBZT Fibers

PBZT (poly (paraphenylene benzobisthiazole)) is first developed in Air Force Material Laboratory. HT PBZT has a tensile strength and modulus of 4.1 GPa and 324 GPa respectively. The compressive properties of HT PBZT and AS PBZT are given in Tables IX and X respectively.

In this study, the compressive strength values of 0.30 GPa and 0.39 GPa for HT PBZT were obtained from the bending beam test and the elastica loop test respectively. They are comparable to the composite compressive strengths of 0.26-0.41 GPa . Also DeTerasa [8] found a compressive strength value of 0.27 GPa for HT PBZT in the bending beam test. But the values given in reference [15] are higher. The elastica loop test results obtained in this study are lower than those given in the table II.

Figure 33 and 34 show the ratio of major to minor (L/D) against major axis (L) for HT PBZT and AS PBZT respectively.

Figure 35 and 36 give the pictures of typical kink bands in HT PBZT at different strain values as observed by optical microscope in the bending beam test.

Scanning electron microscopy method in the elastica test was applied for these fibers as explained in section 3.1.2. The critical strain values obtained in this method show a good agreement with those obtained by optical microscopy method. (See Table I).

Figure 37 shows the typical kink bands in HT PBZT at

different strain levels as observed by scanning electron microscope. These kink bands were observed on the same loop. The picture (a) represents the critical kink band with a critical strain value of 0.104 %. This strain value was calculated by using the radius of circle method explained in the section 3.1.4. The picture (c) shows a kink band at a strain value of 0.196 % , which is two times higher than the critical one. Consequently, we see bigger kink band in the fiber.

Figure 38 (a) shows the critical kink bands at the bottom of the loop as observed by optical microscope. Figure 38 (b) shows the bottom of the loop after the loop was collapsed. The pictures in Figure 39 show typical surface irregularities and kink bands in AS PBZT as observed by optical microscope in the bending beam test. As you can see in picture (a) , the surface irregularities seem like kink bands, therefore it was not possible to measure the critical compressive strain in AS PBZT by bending beam method. However the elastica loop test gave the critical strain for AS PBZT because, in this case, the kink bands occur at the compression side of the fiber as shown in Figure 40 (a). Figure 41 shows a surface irregularity on AS PBZT fiber as observed by scanning electron microscope.

Table IX. Compressive Properties of HT PBZT

MODULUS (Tensile Modulus)	E(GPa)	303.0
STRENGTH		
→ Bending beam test	σ_c(GPa)	0.30
→ Elastica loop test	σ_c(GPa)	0.33 - 0.39
→ Composite [15]	σ_c(GPa)	0.26 - 0.41
CRITICAL STRAIN		
→ Bending beam test	e_{cr}(%)	0.100 $\pm$ .050
→ Elastica loop test	e_{cr}(%)	0.110 $\pm$ .020 0.130 $\pm$ .010
→ Composite	e_{cr}(%)	-

Table X. Compressive Properties of AS PBZT

MODULUS (Tensile Modulus)	E(GPa)	110.0
STRENGTH		
→ Bending beam test	σ_c(GPa)	-
→ Elastica loop test	σ_c(GPa)	0.14 - 0.17
→ Composite	σ_c(GPa)	-
CRITICAL STRAIN		
→ Bending beam test	e_{cr}(%)	-
→ Elastica loop test	e_{cr}(%)	0.130 $\pm$ .010 0.150 $\pm$ .010
→ Composite	e_{cr}(%)	-

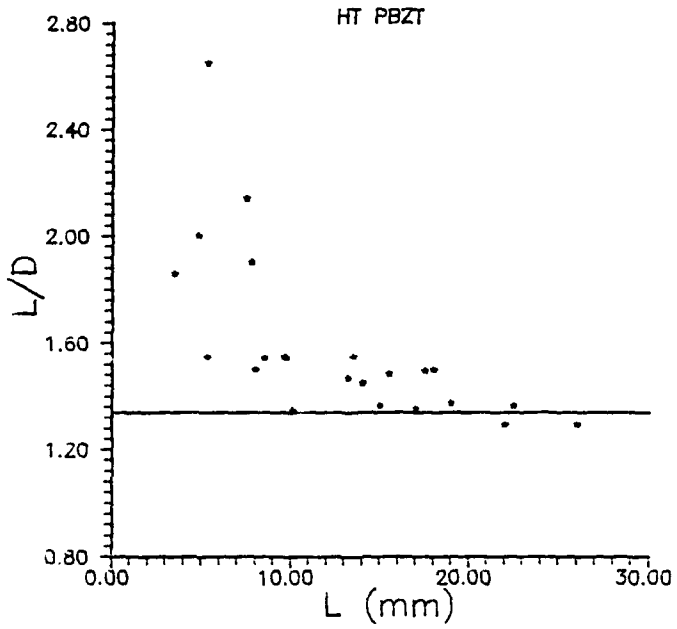

Figure 33. Ratio of Major to Minor Axis (L/D) against Major Axis (L) for HT PBZT Fibers.

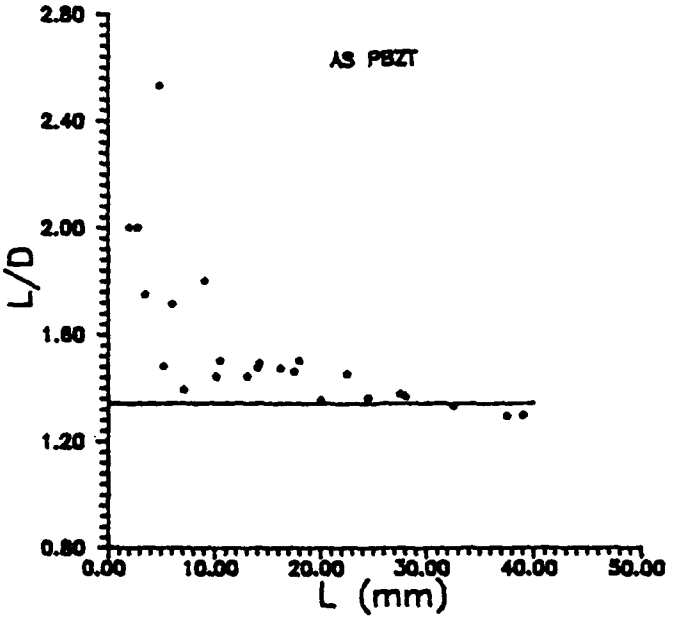

Figure 34. Ratio of Major to Minor Axis (L/D) against Major Axis (L) for AS PBZT.

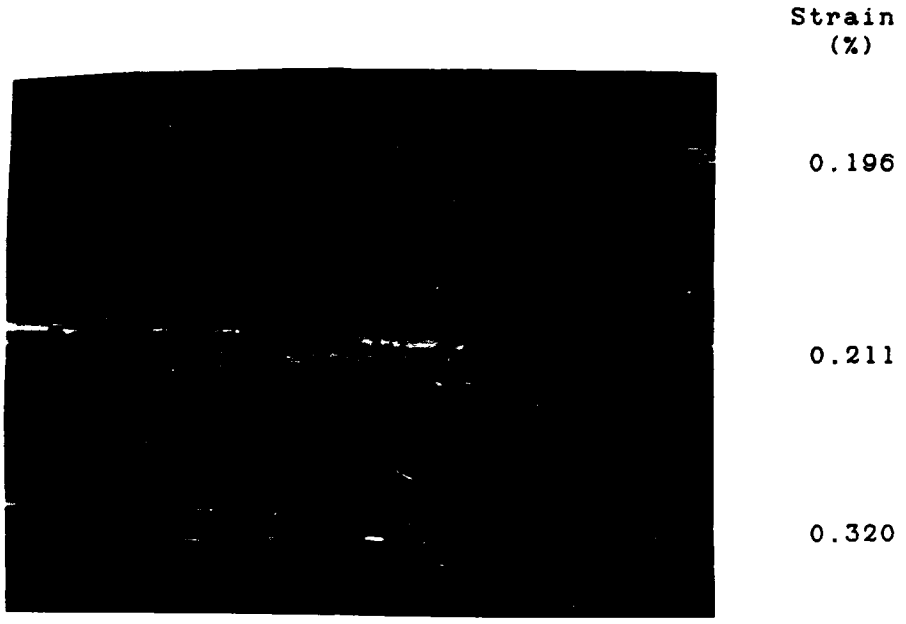

Figure 35. Kink Bands in HT PBZT fiber as observed by Optical Microscope.(The same Portion Of the Fiber) (400X)

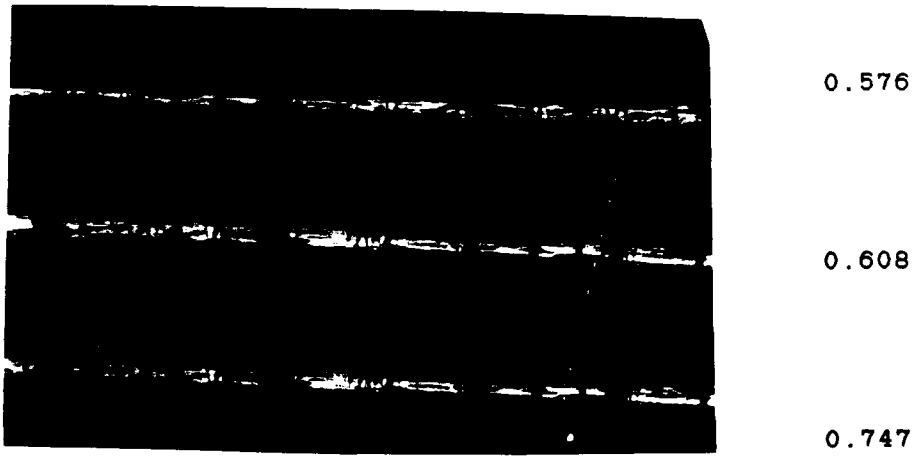

Figure 36. Kink Bands in HT PBZT fiber as observed by Optical Microscope (The same Portion of the Fiber((200X)

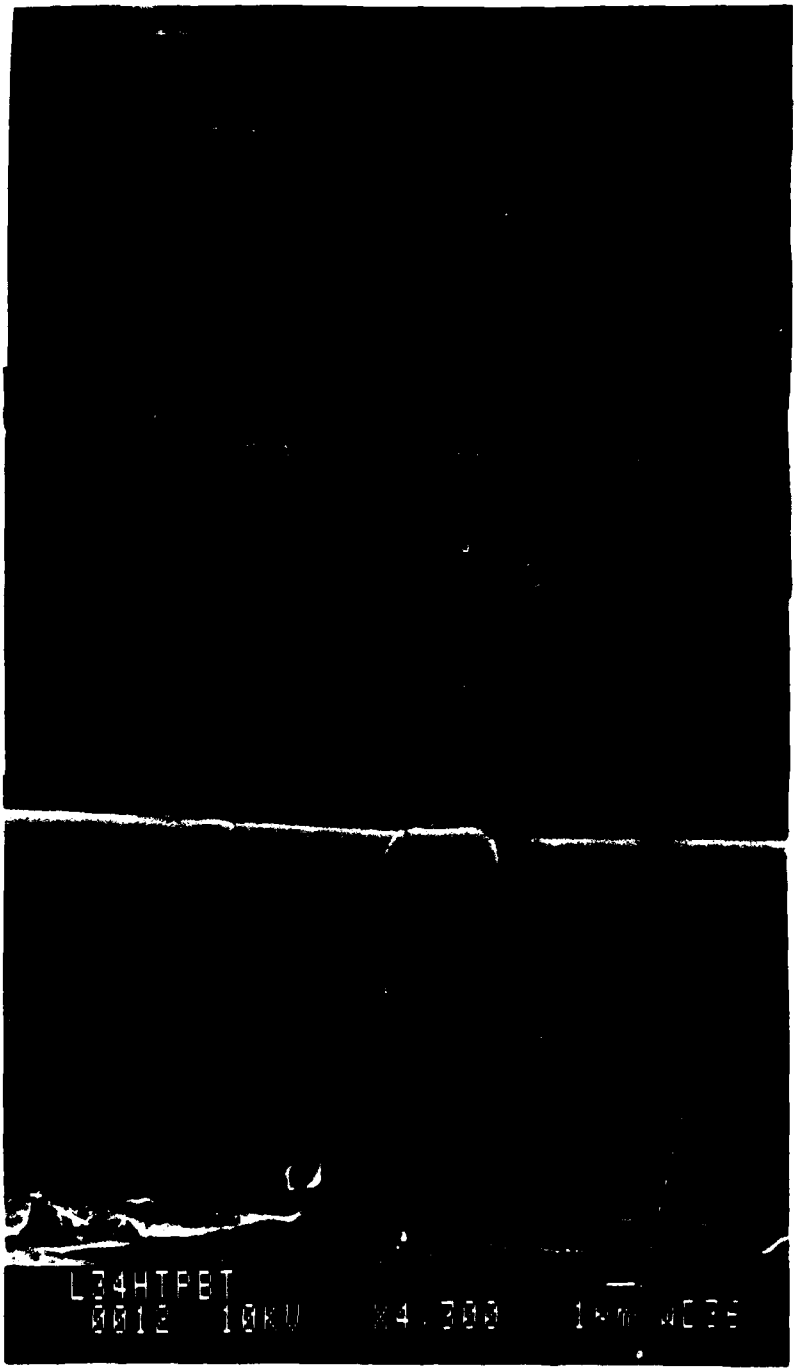

(a)
0.104 %

(b)
0.200 %

(c)
0.196 %

Figure 37. Kink Bands in the HT PBZT Fiber as observed by Scanning Electron Microscope.

(a)

(b)

Figure 38. (a) The Critical Kink Bands in HT PBZT at the bottom of the loop in the elastica loop test.
(b) The Bottom of the Loop after the Loop was collapsed.

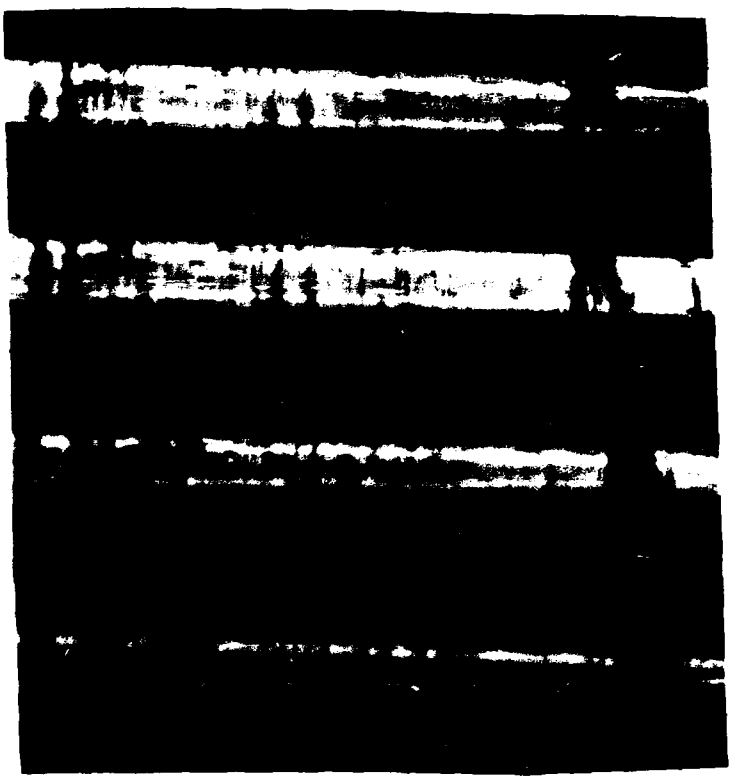

Figure 39. Surface Irregularities and Kink Bands in AS PBZT as observed by Optical Microscope in the Bending Beam Test. (400X)

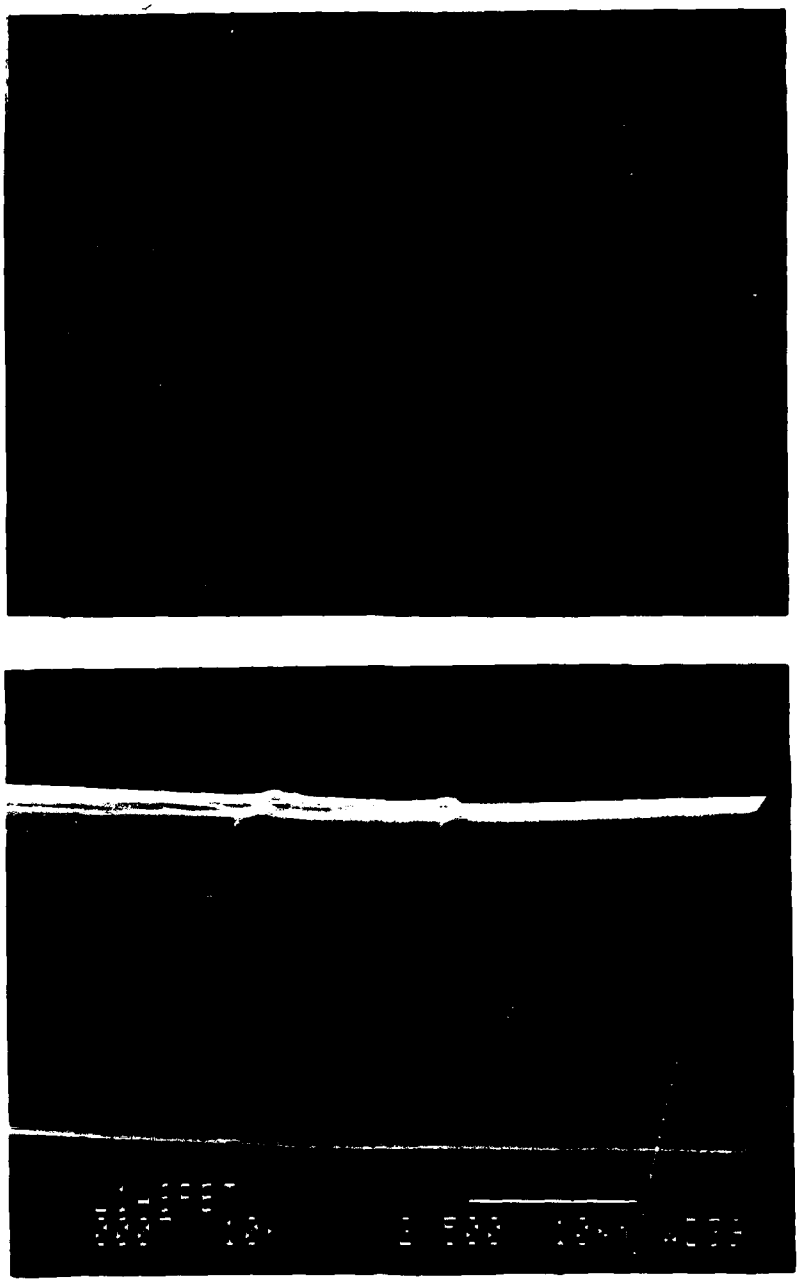

(a)

(b)

Figure 40. (a) Kink Bands in the AS PBZT at the Bottom of Loop as observed by Optical Microscope
(b) Kink Band in AS PBZT as observed by Scanning Electron Microscope.

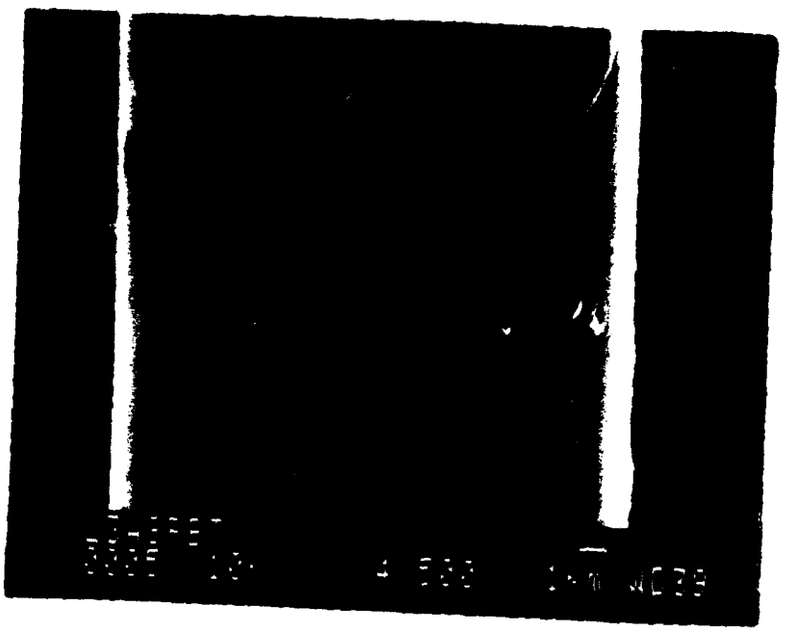

Figure 41. Surface Irregularities on the AS PBZT fiber as observed by Scanning Electron Microscope.

4.4.6 Compressive Behavior of Carbon Fibers

Only bending beam test has been performed on three carbon fibers: T-50, T-300 and P-75S. The criteria for measuring the critical strain in the carbon fibers was different than the one used in the polymer fibers. Here, the last fracture in the carbon fiber was observed by optical microscope, whereas in polymeric fibers, the last kink band was detected. Since the carbon fibers are opaque, the only detectable deformation mode in the fiber was the cracked surfaces or shear dislocation of the fiber due to the fracture. (See Figures 42 and 43, and refer to Section 3.2)

Table XI and Table XII give the compressive properties of T-50 and P-75S carbon fibers respectively. For T-300 carbon fiber, up to the compressive strain limit of the bending beam test because no fracture or observable deformation in the fiber has been detected. It was expected that the critical strain value would be higher than those of T-50 and P-75s. Kumar [15] reported that the significant reduction in compressive strength with increased modulus was observed in carbon fibers. T-300 carbon fiber has a tensile modulus of 234 GPa, which is lower than those of T-50 and P-75S.

(a)

(b)

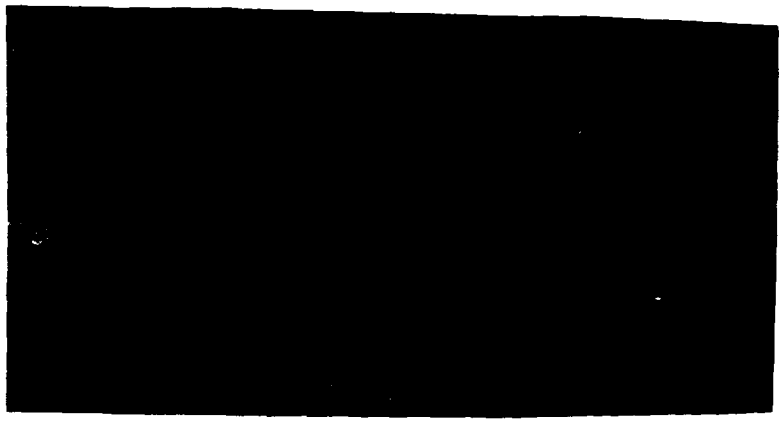

Figure 42. T-50 fiber (a) Before bending
(b) After bending, Fracture Surfaces (200X)

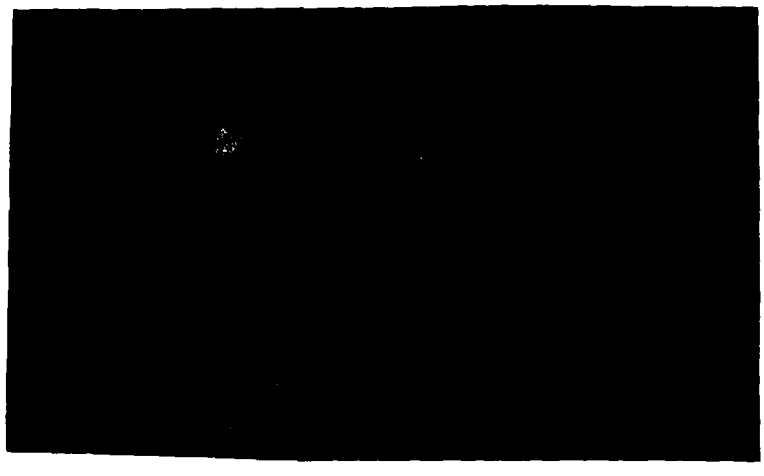

Figure 43. Fracture Surfaces in P-75S Fiber under Compression Stresses (200X)

Table XI. Compressive Properties of T-50 Carbon Fibers

MODULUS (Tensile Modulus)	E(GPa)	393.0
STRENGTH		
→ Bending beam test	σ_c(GPa)	4.09
→ Elastica loop test	σ_c(GPa)	-
→ Composite [15]	σ_c(GPa)	1.61
STRAIN TO FRACTURE		
→ Bending beam test	e_{cr}(%)	1.040 $\pm$ .080
→ Elastica loop test	e_{cr}(%)	-
→ Composite	e_{cr}(%)	-

Table XII. Compressive Properties of P-75S Carbon Fibers

MODULUS (Tensile Modulus)	E(GPa)	517
STRENGTH		
→ Bending beam test	σ_c(GPa)	2.69
→ Elastica loop test	σ_c(GPa)	-
→ Composite	σ_c(GPa)	-
STRAIN TO FRACTURE		
→ Bending beam test	e_{cr}(%)	0.520 $\pm$ .070
→ Elastica loop test	e_{cr}(%)	-
→ Composite	e_{cr}(%)	-

4.5 Comparison of the Results of Bending Beam and Elastica Loop Test

A comparison of these two test results is difficult in terms of the volume of material subjected to the risk of failure in bending beam and elastica loop test. In bending beam tests, the axial stresses are applied through the fiber and in elastica loop test, the pure bending moment is applied to the fiber. Therefore the bending beam test loads the whole fiber section, while the elastica loop test concentrates the stresses at a small area on the surface. Hence, it is expected that the elastica loop test result will be slightly higher than those of bending beam test. The results in table I showed that this expectation is true for PBO and PBZT fiber. It seemed that it didn't hold for Kevlar™ fibers; but a careful observation is required here. If you look at the columns of e_{cr} for elastica loop test, you will see two separate sections under optical microscopy method: minimum radius and elastica. These are the two separate methods to calculate the critical strain from the same loop test. (Refer to Section 3.1.4.). Minimum radius critical strain value is higher than that of elastica value and consequently, it is higher than the one obtained from the bending beam test. Therefore, expecting higher strength values from elastica loop test than from bending beam test holds for Kevlar™ fibers too. The section 4.3.3 in reference [26] , about comparison between tensile and

flexure strength shows clear support about the argument above. In this study, Weibull statistical strength theory was used in conjunction with composite materials to show that,the flexure test could produce significantly higher tensile strengths than the tensile test.

CHAPTER V

5. CONCLUSIONS AND RECOMMENDATIONS

5.1 Conclusions

The following conclusions can be made from this thesis:

1. Two single filament compression test methods - the elastica loop test and bending beam test - were conducted successfully for the polymeric and carbon fibers to measure their compressive properties. Generally, compressive strengths of fibers obtained from these techniques are slightly higher than those obtained from the composite compression test methods. It is believed that this is because of the different test methodologies applied. It can be concluded that these two techniques can give good predictions in measuring the compressive properties of the fibers.

2. The compressive failure mode in polymeric fiber was observed as kink band formation while the compressive failure mode in carbon fibers was detected as fracture. In literature, there are two theories to give the mechanisms for the kink band formation: one says that kink band formation results from the buckling and separation of microfibrils due to elastic instabilities under compression stresses; while the other says that kink band formation is due to the molecular level deformation of the fiber

material. This study tries to model a concept of growing kink band formation starting from the critical kink band which is just the initiation of elastic instabilities, which results in the buckling and separation of microfibrils. It is observed that the critical kink bands disappeared if the load is released at this stage. It is found that, increase in compressive strains in the fiber results in the growing kink band in such a manner that it gets darker and wider. If the load is released at this stage, the shadow of the core of the kink band remains apparent while the big portion of the kink band disappears. It is believed that, this shows the kink band goes under the molecular level deformation at the higher strains than the critical strains, which all fiber compressive properties are based on.

3. Only bending beam test was applied for carbon fibers. Since the observable compressive failure mode in these fibers is fracture, applying the elastica loop test was very difficult in terms of getting the loop dimensions just before the fracture.

4. In bending beam test, kink band formation in Kevlar™ 149 fibers and any fracture in T-300 fibers could not be detected. It is expected that their compressive strengths are higher than the other fibers studied in this thesis.

5. Some fiber surface imperfections make it impossible to observe critical kink band observations by optical microscope. For instance, AS PBZT had such surface

irregularities so that it was not possible to di- inguish the critical kink bands with surface imperfections.

6. The axial stress gradient created along the fiber in the bending beam test is very advantageous in observing the fiber compressive behavior at different stress levels. This axial stress gradient can be changed easily by varying the wedge size or by moving the wedge close to clamped edge.

7. It was found that in-situ observations of fiber deformations under compression is very useful in examining the fiber compressive behavior.

8. It is concluded that the deviations slightly from elastic (L/D) ratio of 1.34 at critical loop stages in the elastica loop test doesn't change the final compressive strain values drastically.

9. Scanning electron microscopy measurements of elastica loop test can be an alternative to optical microscopy because it is believed that it is possible to see very small kink band formations with scanning electron microscopy, which are not detectable with optical microscopy.

10. Elastica shooting test as a potentially new single filament compression test method was developed in this study. Motivation for this study was to make the tests much more simpler and to put into application of numerical analysis of elastica problems to get more sensitive results from the compression tests. This test is open for further

developments including the automatic interaction of the computer with optical microscope and test apparatus, the visual display of deformed fiber and even inclusion of non-linear material properties. It has been demonstrated that the results obtained from this test is very comparable to the ones obtained from elastica loop test for HT PBO fibers.

5.2 Recommendations

The following ideas are recommended for further studies:

1. In many studies including this thesis, it is observed that the kink band formation starts in a region close to fiber surface. This may result from compressive shear forces at the fiber-matrix interface (note that the maximum compressive strain of the fiber is much less than that of the matrix, in our case, of bonding material) and from the lack of transverse coupling between fibrils or microfibrils. This fact can be investigated further by observing the peeled back of fibers at the deformed regions with scanning electron microscopy.

2. Another useful information about the fiber behavior under the tensile forces, can be obtained by taking the fiber off the beam after application of bending beam test and measuring the tensile strength of this fiber by using Instron machine. This measurement will give us an

information about how much compressive deformation will affect the tensile properties of the fiber. Figure 44 gives a schematic for application of above idea. This tensile test will give tensile properties of a compressively deformed fiber. Also a valuable information can be obtained by looking at the tensile fracture point along the fiber after tensile test and matching that point with compressive strain distribution curve as shown in Figure 44. This compressive strain value and the tensile force which causes tensile fracture at that point in fiber will compose further step in investigation of fiber behavior under compression and tensile forces applied alternately.

3. The thicker beam in bending beam test must be used in measurement of compressive properties of Kevlar™ 149 and T-300, so that more compressive strains can be applied to these fibers.

4. Scanning electron microscopy method in elastica loop test can be applied to other fibers to get a good comparison with the optical microscopy method.

5. The elastica shooting test can be developed further for more simple and sensitive measurements of fiber compression or tensile properties. This test must incorporate with sensitive apparatus which applies bending forces to the fiber and holds the fiber at bent position without changing the boundary conditions at one end.

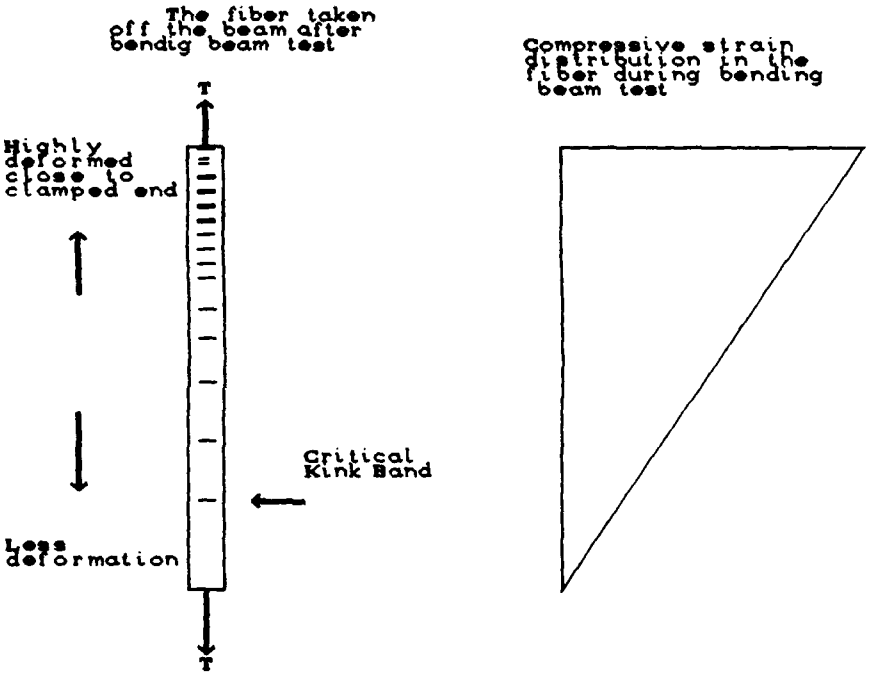

Figure 44. Application of Tensile Test on the Compressively Deformed Fibers by using Instron Machine.

BIBLIOGRAPHY

1. Wilfong, R. E. and J. Zimmerman "Strength and durabilty characteristics of Kevlar Aramid Fiber," Journal of Applied Polymer Science: Applied Polymer Symposium 31.4-21: 1-21 (1977).

2. Greenwood, J. H. and P.G. Rose "Compressive Behaviour of Kevlar 49 Fibers and Composites," Journal of Materials Science, 9: 1809-1814 (1974).

3. Sinclair, David "A Bending Method for Mesurement of the Tensile Strength and Young's Modulus of Glass Fibers," Journal of Applied Physics, 21: 380-386 (1950).

4. Jones, W. R. and J. W. Johnson "Intrinsic Strength and Non-Hookean Behaviour of Carbon Fibers," Carbon, 9: 645-655 (1971).

5. Dobb, M. G. , D. J. Johnson and B. P. Saville "Compressional Behaviour of Kevlar Fibers," Polymer, 22: 960-965 (1981).

6. Allen, S. R. Mechanical and Morphological Correlations in Poly(P-Phenylenebenzobibthiazole) Fibers. Ph.D. *Dissertation*. *Polymer* Science and Engineering Deparment, The University of Massachusetts, 1983.

7. van der Zwaag, S. and G. Kampschoer "Compressive Failure in the High Modulus Polymeric Fibers," Proceedings of the Second International Meeting on Polymer Science and Technology, edited by P. J. Lemstra and L. A. Kleintjens, Elsevier Aplied Science (April 1987).

8. DeTerasa, S. J. The Axial Compressive Strength of High Performance Polymer Fibers. *Ph.D. Dissertation*. Polymer Science and Engineering, University of Massachusetts, March 1985.

9. Parry, T. V. and A. S. Wronski "Kinking and Compressive Failure in Uniaxially Aligned Carbon Fibre Composite Tested Under Superposed Hydrostatic Pressure," Journal of Materials Science, 17: 893-900 (1982).

10. Gurdal, Z. and R. T. Haftka "Compressive Failure Model for Anisotropic Plates with a Cutout," AIAA Journal, 25 (11): 1476-1481(1987).

11. van der Zwaag, S., S. J. Picken and C. P. van Sluijs "Kinkband Formation in Aramid Filaments," Proceedings of the Third International Meeting on Polymer Science and Technology, edited by P. J. Lemstra and L. A. Kleintjens, Elsevier Applied Science (April 1988).

12. Adams, W. W. and R. K. Eby "High-Performance Polymer Fibers," MRS Bulletin: 22-26 (Nov./Dec. 1987).

13. Margolis, J. M. Advanced Thermoset Composites. New York: van Nostrand Reinhold Company, 1986.

14. Hull, D. An Introduction to Composite Materials. Cambridge , Great Britain: Cambridge University Press,1981.

15. Kumar, S. "Structure and Properties of HighPerformance Polymeric and Carbon Fibers- An Overview," Fiber Producers Conference Proceeding,Greenville, S. C.: (April 26-28 / 1988).

16. Keller, R. L., A. N. Palazotto, and S. J. Bai "The Consideration of Compressive Deformation in Polymer Fibers," 28th Structures, Structural Dynamics and Materials Conference, AIAA/ASME/ASCE/AHS : 245-251 (April 6-8, 1987).

17. (a) Kumar, Satish Private Communication.
(b) DuPont Technical Literature on Kevlar (E-95614),(E-95612 6/87).

18. Drzal, L. T. The Interfacial And Compressive Properties of Polybenzothiazole Fibers. Final Report (AFWAL-TR-86-4003), Materials Laboratuary, AFWAL, WPAFB. (1894).

19. Takahashi, T. , M. Miura and K. Sakurai "Deformation Band Studies of Axially Compressed Poly(p-Phenylene Terephthalamide) Fiber," Journal of Applied Polymer Science, 28: 579-586 (1983).

20. Hawthorne, H. M. and E. Teghtsoonian "Axial Compression Fracture in Carbon Fibers," Journal of Materials Science, 10: 41-51 (1975).

21. Allen, S. R. "Tensile Recoil Measurement of Compressive Strength For Polymeric High Performance Fibers," Journal of Materials Science, 22: 853-859 (1987).

22. Kumar, S. ,W. W. Adams and T. E. Helminiak "Uniaxial Compressive Strength of High Modulus Fibers for Composites," Journal of Reinforced Plastics and Composites, 7: 108-119 (March 1988).

23. Miller, R. E. "Numerical Analysis of a Generalized Plane Elastica," International Journal for Numerical Methods in Engineering, 15: 325-332(1980)

24. Coulter A. B. and R. E. Miller "Numerical Analysis of a Generalized Plane ' Elastica ' with Non-linear Material Properties," International Journal for Numerical Methods in Engineering, 26: 617-630 (1988)

25. Sawyer C.L. "Structure-Property Relations of Liquid crystalline Polymers," International Fiber Journal, 2: 27-30 (March 1987)

26. Whitney M. J., I. M. Daniel and R. B. Pipes Experimental Mechanics of Fiber Reinforced Composite Materials. Society for Experimental Mechanics, No.4 New Jersey: Printice-Hall, Inc. 1984.

APPENDIX -A

Test Equipment List

1. JEOL
   JSM-840 Scanning Microscope
   I.D.NO: MX3312

2. BALZERS
   Mini Deposition System MED010
   I.D.NO: MI 3305
   Balzers QS G 301
   Quartz Crystal Thickness Monitor (MX3310)

3. LEITZ
   Ortholux II POL - BK
   Polarizing Microscope
   6650 P552000

   Leitz Vario-Orthomat
   Camera System for Automatic Photomicrography

4. NIKON
   METAPHOT
   Metallurgical Microscope
   I.D.NO: MP3502

5. BAUSCH & LOMB
   Stereo Zoom 7 Microscope
   I.D.NO: MA2436

   Bausch & Lomb
   AX-1 Automatic Exposure Controller
   I.D.NO: MP3334

   Bausch & Lomb Camera

APPENDIX-B

Elastica Shooting Test

Introduction

Elastica shooting test, potentially a new technique for testing the single fibers under compression is developed in this study. The test incorporates with a FORTRAN program and single fiber test results in which a fiber is bent with large displacements. The FORTRAN program has been written for analysis of continuous flexible members. Since the large deformations are anticipated, the shooting method [23] is used along with a Newton-type iteration. In this method, the geometry might be non-linear but fiber behavior remains linear elastic.

The test uses the same criteria with the elastica loop and bending beam test in terms of assumptions made: that the fiber is elastic until the first kink bands are observed in the fiber. Therefore, the fiber is bent until the first kink bands are seen near the clamped end as shown in Figure B-1. Initial and final positions of the fiber are recorded for use in the FORTRAN program. The end displacements, x_p and y_p are used for iterative purposes. In our iteration, P is guessed and the shooting method is applied to reach x_p and y_p displacements obtained from the experiment. This

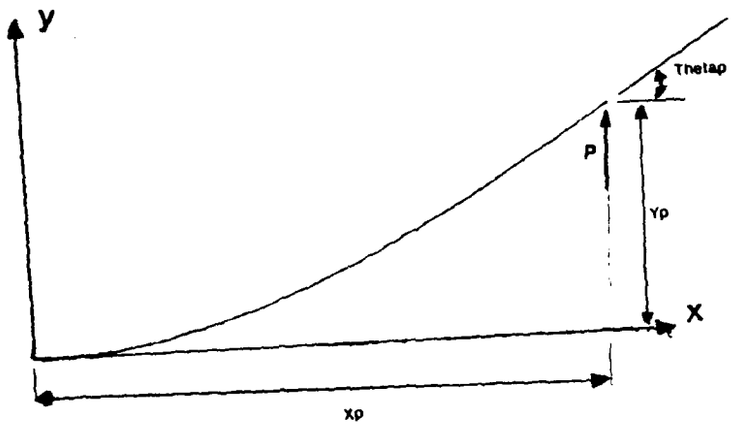

Figure B-1 Schematic of Elastica
Shooting Technique

iteration continues with small increments of P until x_p and y_p are reached. At this time it is possible to calculate stresses and strains at each element which the fiber is divided into.

The next section explains the *elastica shooting* method and the FORTRAN program in detail. The last section includes the application of this new technique and the future improvements.

Shooting Method

This method is reported in references [23] and [24] in detail. The studies will be summarized here for reader's convenience.

The shooting method is a straightforward approximation procedure for the numerical analysis of a continuous flexible member. A continuous member may have an arbitrary shape and loading as shown in Figure B-2. External force and couples can be applied at the points along the member as well as the end points.

The member may be non-uniform but the cross-section dimensions are small compared to the length. Bending and axial deformations of the member are included in the analysis. Displacements can be large but the strains must be small and the material behavior must remain linear elastic.

Problem formulation includes:

(a) Initial geometry and material properties

(b) Division into elements including initial

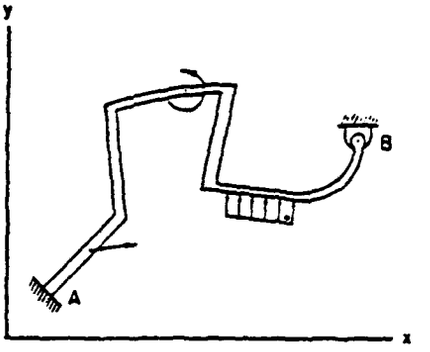

Figure B-2 Continuous Member with Arbitrary Shape and Loads.

coordinates of all node points

(c) Applied external forces and moments at node points

(d) Three boundary conditions at each end

The position of each node point and orientation of the following element are determined in terms of the position of the preceding node and the deformation of the element between two nodes. Also the elements are considered to remain straight between nodes.

Let's assume that six variables (Fx, Fy, C, X, Y, θ) are known at the left end A as shown in Figure B-1. Since all variables are known the iteration is not needed for this case. If the three variables out of six are known at end A, the iteration procedure should be conducted (refer to [23]).

a) The following equations will be used to obtain P_i, V_i, M_i for the ith element. (See Figure B-3)

$$P_i = - \left(\sum_{j=1}^{i} Fx_j \right) \cos \theta_i - \left(\sum_{j=1}^{i} Fy_j \right) \sin \theta_i \qquad (1)$$

$$V_i = - \left(\sum_{j=1}^{i} Fx_j \right) \sin \theta_i + \left(\sum_{j=1}^{i} Fy_j \right) \cos \theta_i \qquad (2)$$

$$M_i = - \sum_{j=1}^{i} C_j + \sum_{j=1}^{i-1} \left[Fy_j \, (x_i - x_j) - Fx_j \, (y_i - y_j) \right] \qquad (3)$$

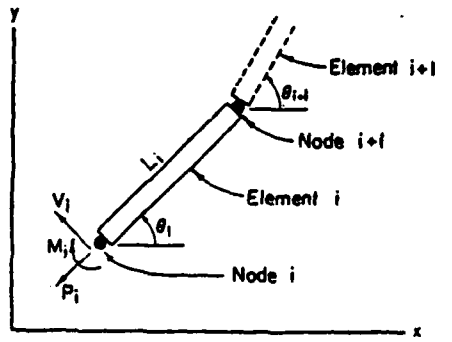

Figure B-3 Typical Element Representation of Continuous Member.

where P_i, V_i, and M_i are internal axial load, shear load and bending moment respectively. θ_i is the orientation angle of the i th element after deformation.

b) To obtain the loaded length of the element:

$$L_i = L_{io} \left(1 + \frac{P_i}{A_i E_i} \right) \tag{4}$$

where L_{io}, E_i, A_i are the original length, Young's modulus and cross-sectional area of ith element.

c) The coordinates of the $(i+1)$th node:

$$x_{i+1} = x_i + L_i \cos\theta_i \tag{5}$$

$$y_{i+1} = y_i + L_i \sin\theta_i \tag{6}$$

d) The relative change in slope between two ends of the element:

$$\phi = \left(M_i + \frac{P_i L_i}{2} \right) \frac{L_i}{E_i I_i} \tag{7}$$

where I_i is the moment of inertia.

e) To obtain the angular orientation of the $(i+1)$ th element:

$$\theta_{i+1} = \theta_i + (\theta_{i+1o} - \theta_{io}) + \phi_i \tag{8}$$

where θ_{i+1o} and θ_{io} are the original orientation angles of the ith and $(i+1)$th elements.

FORTRAN Program

The FORTRAN program has 306 statements, 6 subroutines and four external files. It has been written by using Microsoft® FORTRAN for personal computers.

Besides the main program, the following subroutines are included in the program: subroutine data, which reads the parameters from the external data files; subroutine anlys, which uses the equations on the pages 111 and 113; subroutine iter, which is for iteration if three parameters out of six are known at one end of the member; subroutine equil, which is used for getting overall equilibrium of loads on the member; subroutine write, which is for getting a hard copy of results and the data required to plot the deformed member.

The following external files are used in the program:

Data 1 is used for reading the material properties and geometry such as cross-sectional area (AR), the moment of inertia (IM), the Young's modulus (E) and the fiber radius (R). Also the deformed member coordinates of the end B from experimentation, and the forces and moments applied at the end A, (See Figure B-1) are given in this file.

Data 2 is used for reading the initial coordinates of the member.

Result 1 is used for a hard copy of results obtained after analysis, which includes the coordinates of the deformed body, forces, moments, and strains at each node.

Result 3.DAT is used for storing data required for

visual display of the deformed member by using GRAPHER, which is a product of Golden Software Inc.,1988.The FORTRAN code and sample output (from the file, result1) are given in the appendix C.

Application

This test method was conducted for only HT PBO (5% NH_4OH), which was produced in the materials laboratory. The fiber was deflected at one end while the other end was fixed with carbon cement, as shown in Figure B-4. Special care was taken in applying the force in the y-direction. Since this force was applied by hand, it was one of the drawbacks of the test. The other point that we have to consider is that the deflected end was fixed with glue to observe the deformation in the fiber under microscope. This was the second drawback of the test. However, they can be easily corrected by making an apparatus to bend the fiber and hold the fiber in the bent position under microscope.

The Figure B-4 (a) and (b) show the fiber on the horizontal glass cover before bending and after bending respectively. Note that the fiber was bent until the first kink bands were seen near the clamped edge of the fiber as seen in Figure B-5. At this position , a picture of bent fiber was taken. From this picture , x_p , y_p and thetap can be found as:

$$X_p = 5.52 \text{ mm}$$

$$y_p = 2.35 \text{ mm}$$

$$\text{Thetap} = 0.52 \text{ rad}$$

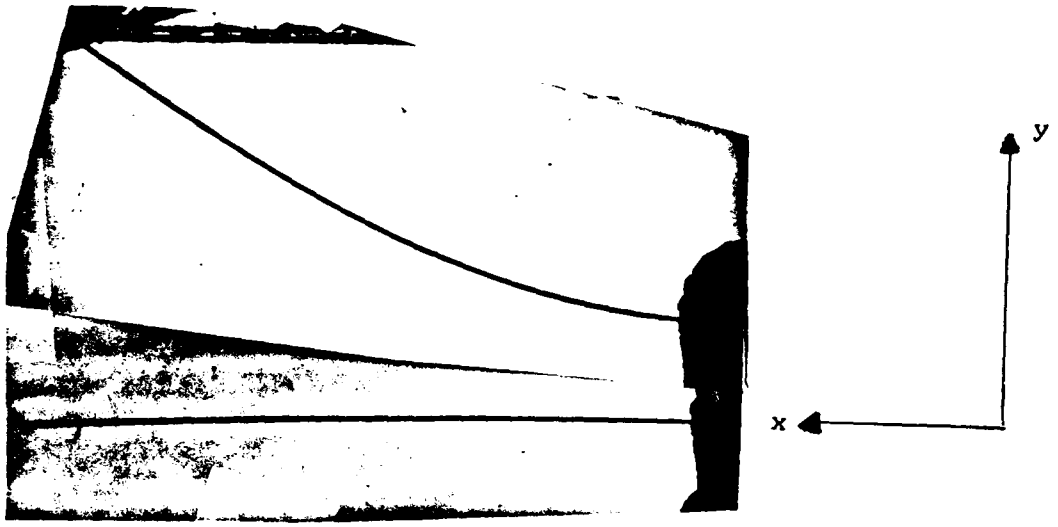

Figure B-4 Pictures of the fiber before and after bending in the elastica shooting technique.

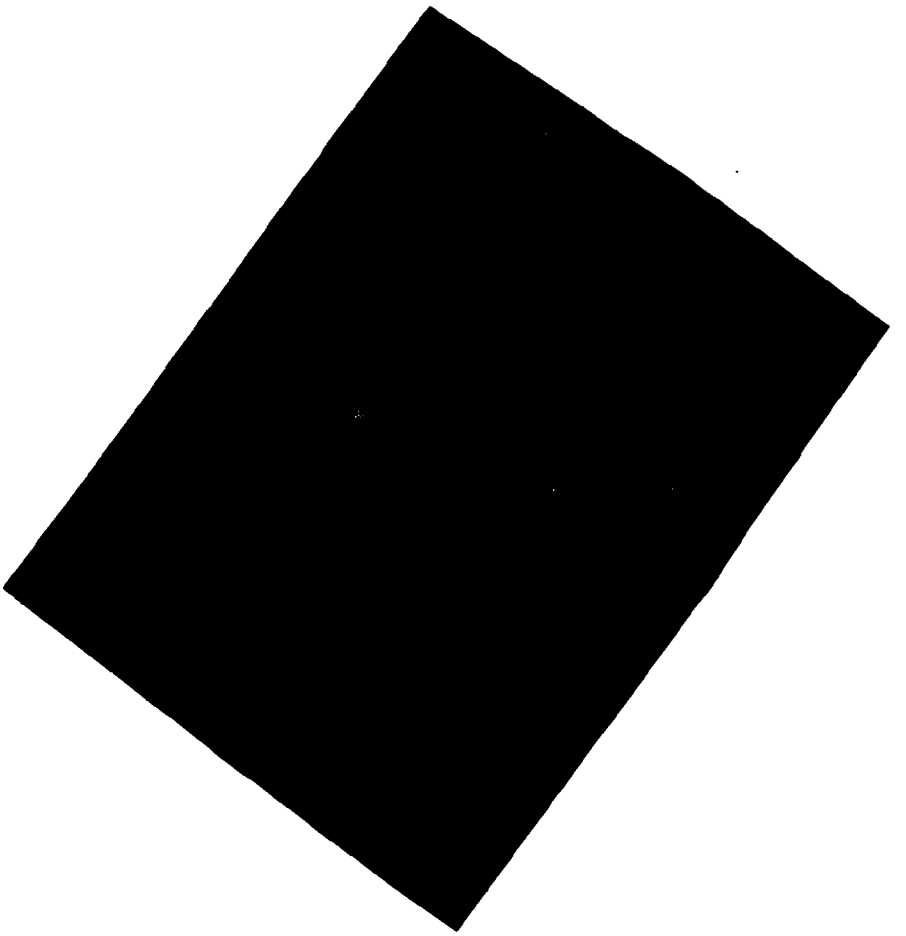

Figure B-5 The first Kink Bands near the Fixed Edge as observed from Optical Microscope. (X250)

These values are given the program through the external file: Datal. These are the values that we are shooting in the FORTRAN program. Since the only force in y direction was applied, we should reach the Xp value first. And the others would be found automatically.

The fiber was divided into 71 elements (72 nodes), given in Data2. The fiber geometry and material properties are given in external file, Datal. These are:

Cross-section Area (AR) = $.683 \times 10^{-9}$ mm^2

Young's Modulus (E) = 0.372×10^{-7} N/mm^2

Moment of Inertia (IM) = 1.5169×10^{5} mm^4

Fiber Radius (R) = 0.015 mm

Also in the Datal, the first estimation of vertical force, Fy(1) at the end A and the force increment for the iteration (FC) are given.

The results of this analysis are given in Result1 file. One page of this file , which shows the compressive strain value (EM) in the first element of the fiber, is given in the appendix C. Note that the compressive strain value near the fixed end of the fiber is 0.2876 %. This value is very comparable with the compressive strain value of 0.31 % obtained form elastica loop test.

The plot of deformed fiber after numerical analysis is given in figure B-6. This plot has the same scale with the deformed fiber in the figure B-4. Note that both curves match each other exactly. This shows the good efficiency of the method.

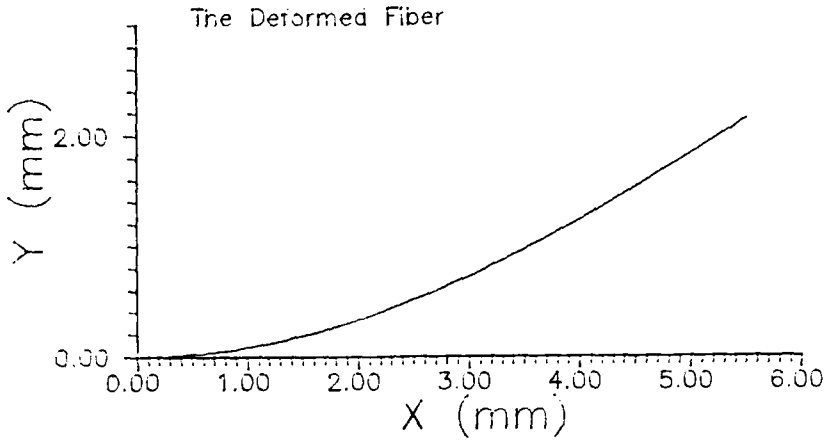

Figure B-6 Plot of the Deformed Fiber as an Output of the FORTRAN Program.

Appendix-C

FORTRAN Code for Elastica Shooting Technique

```
      PROGRAM ELAS
      INTEGER N,NE,A,I,J,K
      REAL*8 X0(100),Y0(100),X(100),Y(100),L0(100),L(100),
     *FY(100),FX2(100),FY2(100),C2(100),
     *FX(100),C(100),P(100),V(100),M(100),THETA(100),
     *THETA0(100),XP,YP,THETAP,
     *PHI(100),OM(100),EP(100),EM(100),AR,IM,E,R,X1,X2,Y1,Y2,
     *THETA1,THETA2,FC
      COMMON X0,Y0,X,Y,L0,L,FY,FX,C,P,V,M,THETA,THETA0,PHI,OM,EP,EM,
     *AR,IM,E,R,N,NE,XP,YP,THETAP,FC
      OPEN (1,FILE='RESULT1')
      OPEN (2,FILE='DATA1')
      OPEN (3,FILE='DATA2')
      OPEN (5,FILE='RESULT3.DAT')
      CALL DATA
  910 CONTINUE
      CALL ANLYS
      IF(X(N) .GT. (XP*0.999) .AND. X(N) .LT. (XP*1.001)) GOTO 7
      IF(X(N) .GT. XP) GOTO 5
      IF(X(N) .LT. XP) GOTO 6
    5 CONTINUE
      FY(1)=FY(1)+FY(1)*FC
      C(1)=FY(1)*XP
      DO 41 K=2,N
      THETA0(K)=0.0
      FX(K)=0.0
      FY(K)=0.0
      C(K)=0.0
   41 CONTINUE
      GOTO 910
    6 CONTINUE
```

```
      FY(1)=FY(1)-FY(1)*FC
      C(1)=FY(1)*XP
      DO 42 K=2,M
      THETA0(K)=0.0
      FX(K)=0.0
      FY(K)=0.0
      C(K)=0.0
   42 CONTINUE
      GOTO 910
C     CALL ITER
    7 CONTINUE
      CALL WRITE
      CALL EQUIL
      END
```

```
      SUBROUTINE DATA
      INTEGER N,NE,A,I,J,K
      REAL*8 X0(100),Y0(100),X(100),Y(100),L0(100),L(100),
     *FY(100),FX2(100),FY2(100),C2(100),
     *FX(100),C(100),P(100),V(100),M(100),THETA(100),
     *THETA0(100),XP,YP,THETAP,
     *PHI(100),OM(100),EP(100),EM(100),AR,IM,E,R,X1,X2,Y1,Y2,
     *THETA1,THETA2,FC
      COMMON X0,Y0,X,Y,L0,L,FY,FX,C,P,V,M,THETA,THETA0,PHI,OM,EP,EM,
     *AR,IM,E,R,N,NE,XP,YP,THETAP,FC
C MATERIAL PROPERTIES AND GEOMETRY
      READ(2,109)AR,IM,E,R
  109 FORMAT(E10.3,E10.3,E10.3,F5.3)
C INITIAL COORDINATES
      I=1
   20 CONTINUE
      READ(3,107) X0(I),Y0(I),A
  107 FORMAT(F6.3,F6.3,I1)
      IF(A.EQ.1) GOTO 50
      I=I+1
      GO TO 20
   50 CONTINUE
C NODE NUMBER
      N=I
C ELEMENT NUMBER
      NE=N-1
C ORIGINAL LENGTHS OF ELEMENTS
      DO 40 J=1,NE
      L0(J)=SQRT((X0(J+1)-X0(J))**2+(Y0(J+1)-Y0(J))**2)
      THETA0(J)=ATAN((Y0(J+1)-Y0(J))/(X0(J+1)-X0(J)))
   40 CONTINUE
C PRESCRIBED VALUES
      X(1)=X0(1)
```

```
      Y(1)=YO(1)
      THETA(1)=THETAO(1)
      READ(2,51) XP,YP,THETAP
   51 FORMAT(F6.3,F6.3,F6.3)
C ASSUMED VALUES
      READ(2,52) FX(1),FY(1),FC
   52 FORMAT(E8.2,E8.2,E8.2)
      C(1)=FY(1)*XP
C INITIALIZATION
      DO 41 K=2,N
      FX(K)=0.0
      FY(K)=0.0
      C(K)=0.0
      THETAO(K)=0.0
   41 CONTINUE
      RETURN
      END
```

```
      SUBROUTINE ANLYS
      INTEGER N,NE,A,I,J,K,S
      REAL*8 X0(100),Y0(100),X(100),Y(100),L0(100),L(100),
     *FY(100),FX2(100),FY2(100),C2(100),
     *FX(100),C(100),P(100),V(100),M(100),THETA(100),
     *THETA0(100),XP,YP,THETAP,
     *PHI(100),OM(100),EP(100),EM(100),AR,IM,E,R,X1,X2,Y1,Y2,
     *THETA1,THETA2,FC
      COMMON X0,Y0,X,Y,L0,L,FY,FX,C,P,V,M,THETA,THETA0,PHI,OM,EP,EM,
     *AR,IM,E,R,N,NE,XP,YP,THETAP,FC
      DO 3 I=1,NE
      FX2(I)=FX(I)
      FY2(I)=FY(I)
      C2(I)=C(I)
    3 CONTINUE
      J=1
      OM(J)=0.0
      DO 1 I=1,NE
      P(I)=-FX(I)*COS(THETA(I))-FY(I)*SIN(THETA(I))
      V(I)=-FX(I)*SIN(THETA(I))+FY(I)*COS(THETA(I))
      IF(I.EQ.1) GOTO 129
      OM(I)=(FY(1)*(X(I)-X(1))-FX(1)*(Y(I)-Y(1)))
  129 CONTINUE
      M(I)=-C(I)+OM(I)
      EP(I)=P(I)/(AR*E)
      EM(I)=(M(I)*R)/(E*IM)
      L(I)=L0(I)*(1+P(I)/(AR*E))
      K=I+1
      FX(K)=FX(K)+FX(I)
      FY(K)=FY(K)+FY(I)
      C(K)=C(K)+C(I)
      PHI(I)=(M(I)+(V(I)*L(I))/2.0)*L(I)/(E*IM)
      THETA(K)=THETA(I)+(THETA0(K)-THETA0(I))+PHI(I)
```

```
      X(K)=X(I)+L(I)*COS(THETA(I))
      Y(K)=Y(I)+L(I)*SIN(THETA(I))
    1 CONTINUE
      DO 2 J=1,NE
```

```
      SUBROUTINE ITER
      INTEGER N,NE,A,I,J,K
      REAL*8 X0(100),Y0(100),X(100),Y(100),L0(100),L(100),
     *FY(100),FX2(100),FY2(100),C2(100),
     *FX(100),C(100),P(100),V(100),M(100),THETA(100),
     *THETA0(100),XP,YP,THETAP,
     *PHI(100),OM(100),EP(100),EM(100),AR,IM,E,R,X1,X2,Y1,Y2,
     *THETA1,THETA2,FC
      REAL*8 G1,G2,G3,H1,H2,H3,G1S,G2S,G3S,H1S,H2S,H3S,
     *DH1G1,DH1G2,DH1G3,DH2G1,DH2G2,DH2G3,DH3G1,DH3G2,DH3G3,
     *F1,F2,F3,GS1K,GS2K,GS3K,GS1,GS2,GS3
      COMMON X0,Y0,X,Y,L0,L,FY,FX,C,P,V,M,THETA,THETA0,PHI,OM,EP,EM,
     *AR,IM,E,R,N,NE,XP,YP,THETAP,FC
      G1=FX(1)
      G2=FY(1)
      G3=C(1)
      H1=X(N)
      H2=Y(N)
      H3=THETA(N)
      G1S=G1+G1*1.E-02
      FX(1)=G1S
      FY(1)=G2
      C(1)=G3
      DO 42 K=2,N
      THETA0(K)=0.0
      FX(K)=0.0
      FY(K)=0.0
      C(K)=0.0
   42 CONTINUE
      CALL ANLYS
      H1S=X(N)
      H2S=Y(N)
      H3S=THETA(N)
```

```
      DH1G1=(H1S-H1)/(G1S-G1)
      DH2G1=(H2S-H2)/(G1S-G1)
      DH3G1=(H3S-H3)/(G1S-G1)

      G2S=G2-G2*1.E-02
      FX(1)=G1
      FY(1)=G2S
      C(1)=G3
      DO 43 K=2,N
      THETA0(K)=0.0
      FX(K)=0.0
      FY(K)=0.0
      C(K)=0.0
   43 CONTINUE
      CALL ANLYS
      H1S=X(N)
      H2S=Y(N)
      H3S=THETA(N)
      DH1G2=(H1S-H1)/(G2S-G2)
      DH2G2=(H2S-H2)/(G2S-G2)
      DH3G2=(H3S-H3)/(G2S-G2)

      G3S=G3+G3*1.E-02
      FX(1)=G1
      FY(1)=G2
      C(1)=G3S
      DO 44 K=2,N
      THETA0(K)=0.0
      FX(K)=0.0
      FY(K)=0.0
      C(K)=0.0
   44 CONTINUE
      CALL ANLYS
```

```
      H1S=X(N)
      H2S=Y(N)
      H3S=THETA(N)
      DH1G3=(H1S-H1)/(G3S-G3)
      DH2G3=(H2S-H2)/(G3S-G3)
      DH3G3=(H3S-H3)/(G3S-G3)
      F1=XP-H1+G1*DH1G1+G2*DH1G2+G3*DH1G3
      F2=YP-H2+G1*DH2G1+G2*DH2G2+G3*DH2G3
      F3=THETAP-H3+G1*DH3G1+G2*DH3G2+G3*DH3G3
      GS1K=0.0
      GS2K=0.0
      GS3K=0.0
  191 CONTINUE
      GS1=(1/DH1G1)*(F1-DH1G2*GS2K-DH1G3*GS3K)
      GS2=(1/DH2G2)*(F2-DH2G1*GS1K-DH2G3*GS3K)
      GS3=(1/DH3G3)*(F3-DH3G1*GS1K-DH3G2*GS2K)
      IF(GS1.EQ.GS1K .AND. GS2.EQ.GS2K .AND. GS3.EQ.GS3K) GOTO 192
      GS1K=GS1
      GS2K=GS2
      GS3K=GS3
      GO TO 191
  192 CONTINUE
      FX(1)=GS1
      FY(1)=GS2
      C(1)=GS3
      DO 41 K=2,N
      THETA0(K)=0.0
      FX(K)=0.0
      FY(K)=0.0
      C(K)=0.0
   41 CONTINUE
      RETURN
      END
```

```
      SUBROUTINE EQUIL
      INTEGER N,NE,A,I,J,K
      REAL*8 X0(100),Y0(100),X(100),Y(100),L0(100),L(100),
     *FY(100),FX2(100),FY2(100),C2(100),
     *FX(100),C(100),P(100),V(100),M(100),THETA(100),
     *THETA0(100),XP,YP,THETAP,
     *PHI(100),OM(100),EP(100),EM(100),AR,IM,E,R,X1,X2,Y1,Y2,
     *THETA1,THETA2,FC
      REAL*8 SUM1(100),SUM2(100),SUM3(100),OMN(100)
      COMMON X0,Y0,X,Y,L0,L,FY,FX,C,P,V,M,THETA,THETA0,PHI,OM,EP,EM,
     *AR,IM,E,R,N,NE,XP,YP,THETAP,FC
      J=1
      SUM1(J)=0.0
      SUM2(J)=0.0
      SUM3(J)=0.0
      OMN(J)=0.0
      DO 50 I=1,NE
      SUM1(I+1)=SUM1(I)+FX(I)
      SUM2(I+1)=SUM2(I)+FY(I)
      SUM3(I+1)=SUM3(I)+C(I)
      OMN(I+1)=OMN(I)+(FY(I)*(X(NE+1)-X(I))+FX(I)*(Y(NE+1)-Y(I)))
   50 CONTINUE
      FX(NE+1)=-SUM1(NE+1)
      FY(NE+1)=-SUM2(NE+1)
      C(NE+1)=-SUM3(NE+1)+OMN(NE+1)
      WRITE(1,123)
  123 FORMAT('OVERALL EQUILIBRIUM')
      WRITE(1,124) FX(NE+1),FY(NE+1),C(NE+1)
  124 FORMAT(1X,'FX(N)=',E10.4,'FY(N)=',E10.4,'C(N)=',E10.4)
      RETURN
      END
```

```
      SUBROUTINE WRITE
      INTEGER N,NE,A,I,J,K
      REAL*8 X0(100),Y0(100),X(100),Y(100),L0(100),L(100),
     *FY(100),FX2(100),FY2(100),C2(100),
     *FX(100),C(100),P(100),V(100),M(100),THETA(100),
     *THETA0(100),XP,YP,THETAP,
     *PHI(100),OM(100),EP(100),EM(100),AR,IM,E,R,X1,X2,Y1,Y2,
     *THETA1,THETA2,FC
      COMMON X0,Y0,X,Y,L0,L,FY,FX,C,P,V,M,THETA,THETA0,PHI,OM,EP,EM,
     *AR,IM,E,R,N,NE,XP,YP,THETAP,FC
      WRITE(1,9)
    9 FORMAT(2X,'NODE',4X,'X0',5X,'X',5X,'Y0',6X,'Y',6X,'THETA')
      DO 20 I=1,N
      WRITE(5,21) X(I),Y(I)
   21 FORMAT(1X,F5.2,2X,F5.2)
   20 CONTINUE
      DO 1 I=1,N
      WRITE(1,10) I,X0(I),X(I),Y0(I),Y(I),THETA(I)
   10 FORMAT(3X,I3,2X,F5.2,2X,F5.2,2X,F5.2,2X,F5.2,2X,F5.2)
   14 FORMAT(1X,E10.3,',',E10.3,',',I1)
   15 CONTINUE
    1 CONTINUE
      WRITE(1,11)
   11 FORMAT(1X,'ELEMENT',4X,'FX',6X,'FY',7X,'P',9X,'V',10X,'M',
     *9X,'EM',10X,'EP')
      DO 2 J=1,NE
      WRITE(1,12) J,FX(J),FY(J),P(J),V(J),M(J),EM(J),EP(J)
   12 FORMAT(2X,I3,2X,E8.2,1X,E8.2,1X,E10.4,1X,E10.4,1X,E10.4,1X,E10.4,
     *1X,E8.2)
    2 CONTINUE
      RETURN
      END
```

ELEMENT	FX(N)	FY(N)	P(N)	V(N)	M(N-mm)	EM
1	.00E+00	-.20E-03	.0000E+00	-.1960E-03	.1082E-02	.2876E-02
2	.00E+00	.00E+00	.1871E-05	-.1960E-03	.1072E-02	.2850E-02
3	.00E+00	.00E+00	.3725E-05	-.1960E-03	.1062E-02	.2824E-02
4	.00E+00	.00E+00	.5561E-05	-.1960E-03	.1053E-02	.2798E-02
5	.00E+00	.00E+00	.7380E-05	-.1959E-03	.1043E-02	.2772E-02
6	.00E+00	.00E+00	.9182E-05	-.1958E-03	.1033E-02	.2746E-02
7	.00E+00	.00E+00	.1097E-04	-.1957E-03	.1023E-02	.2720E-02
8	.00E+00	.00E+00	.1273E-04	-.1956E-03	.1014E-02	.2694E-02
9	.00E+00	.00E+00	.1448E-04	-.1955E-03	.1004E-02	.2668E-02
10	.00E+00	.00E+00	.1621E-04	-.1954E-03	.9940E-03	.2642E-02
11	.00E+00	.00E+00	.1792E-04	-.1952E-03	.9842E-03	.2616E-02
12	.00E+00	.00E+00	.1961E-04	-.1950E-03	.9744E-03	.2590E-02
13	.00E+00	.00E+00	.2129E-04	-.1949E-03	.9647E-03	.2564E-02
14	.00E+00	.00E+00	.2294E-04	-.1947E-03	.9549E-03	.2538E-02
15	.00E+00	.00E+00	.2458E-04	-.1945E-03	.9452E-03	.2513E-02
16	.00E+00	.00E+00	.2620E-04	-.1943E-03	.9355E-03	.2487E-02
17	.00E+00	.00E+00	.2780E-04	-.1940E-03	.9258E-03	.2461E-02
18	.00E+00	.00E+00	.2939E-04	-.1938E-03	.9161E-03	.2435E-02
19	.00E+00	.00E+00	.3095E-04	-.1936E-03	.9064E-03	.2409E-02
20	.00E+00	.00E+00	.3249E-04	-.1933E-03	.8967E-03	.2384E-02
21	.00E+00	.00E+00	.3402E-04	-.1931E-03	.8870E-03	.2358E-02
22	.00E+00	.00E+00	.3553E-04	-.1928E-03	.8774E-03	.2332E-02
23	.00E+00	.00E+00	.3849E-04	-.1922E-03	.8581E-03	.2281E-02
24	.00E+00	.00E+00	.4138E-04	-.1916E-03	.8389E-03	.2230E-02
25	.00E+00	.00E+00	.4419E-04	-.1910E-03	.8197E-03	.2179E-02
26	.00E+00	.00E+00	.4692E-04	-.1903E-03	.8006E-03	.2128E-02
27	.00E+00	.00E+00	.4959E-04	-.1897E-03	.7816E-03	.2078E-02
28	.00E+00	.00E+00	.5218E-04	-.1890E-03	.7626E-03	.2027E-02
29	.00E+00	.00E+00	.5470E-04	-.1882E-03	.7437E-03	.1977E-02
30	.00E+00	.00E+00	.5714E-04	-.1875E-03	.7249E-03	.1927E-02
31	.00E+00	.00E+00	.5951E-04	-.1868E-03	.7061E-03	.1877E-02

Vita

Sukru FIDAN [redacted]

He studied Mechanical Engineering at Middle East Technical University , in Ankara, Turkey, where he graduated in july 1984 with a BS in Mechanical Engineering. He worked at several factories as a research and development engineer. In May 1987, he started his study for a Master of Science in Aeronautical Engineering at the Air Force Institute of Technology.

[redacted]

UNCLASSFIED

SECURITY CLASSIFICATION OF THIS PAGE

REPORT DOCUMENTATION PAGE

Form Approved OMB No. 0704-0188

1a. REPORT SECURITY CLASSIFICATION: UNCLASSFIED	1b. RESTRICTIVE MARKINGS
2a. SECURITY CLASSIFICATION AUTHORITY	3. DISTRIBUTION/AVAILABILITY OF REPORT: Approved for public release; distribution unlimited.
2b. DECLASSIFICATION/DOWNGRADING SCHEDULE	
4. PERFORMING ORGANIZATION REPORT NUMBER(S): AFIT/GAE/AA/88D - 14	5. MONITORING ORGANIZATION REPORT NUMBER(S)
6a. NAME OF PERFORMING ORGANIZATION: School of Engineering; 6b. OFFICE SYMBOL (If applicable): AFIT/ENY	7a. NAME OF MONITORING ORGANIZATION
6c. ADDRESS (City, State, and ZIP Code): Air Force Institute of Technology, Wright Patterson Air Force Base, OH, 45433	7b. ADDRESS (City, State, and ZIP Code)
8a. NAME OF FUNDING/SPONSORING ORGANIZATION: Materials Laboratory; 8b. OFFICE SYMBOL (If applicable)	9. PROCUREMENT INSTRUMENT IDENTIFICATION NUMBER
8c. ADDRESS (City, State, and ZIP Code): Wright Aeronautical Laboratories, Wright Patterson AFB, OH, 45433	10. SOURCE OF FUNDING NUMBERS: PROGRAM ELEMENT NO. / PROJECT NO. / TASK NO. / WORK UNIT ACCESSION NO.

11. TITLE (Include Security Classification): Experimentation and Analysis of Compression Test Methods for High Performance Polymeric Fibers

12. PERSONAL AUTHOR(S): Sukru FIDAN, 1Lt. TUAF

13a. TYPE OF REPORT	13b. TIME COVERED	14. DATE OF REPORT (Year, Month, Day)	15. PAGE COUNT
MS THESIS	FROM _____ TO _____	1988 December	140

16. SUPPLEMENTARY NOTATION

17. COSATI CODES			18. SUBJECT TERMS (Continue on reverse if necessary and identify by block number)
FIELD	GROUP	SUB-GROUP	
11	09		Polymer Fibers, Compression, Elastica, Elastica Loop Bending Beam, Kink Bands, Kevlars

19. ABSTRACT (Continue on reverse if necessary and identify by block number)

Thesis Advisor: Dr. Anthony N. Palazotto
Department of Aeronautics and Astronautics

Abstract on other side.

12 Jan 1989

20. DISTRIBUTION/AVAILABILITY OF ABSTRACT	21. ABSTRACT SECURITY CLASSIFICATION
☒ UNCLASSIFIED/UNLIMITED ☐ SAME AS RPT. ☐ DTIC USERS	UNCLASSFIED

22a. NAME OF RESPONSIBLE INDIVIDUAL	22b. TELEPHONE (Include Area Code)	22c. OFFICE SYMBOL
Anthony N. Palazotto	513-255-3517	AFIT/ENY

DD Form 1473, JUN 86 — Previous editions are obsolete. — SECURITY CLASSIFICATION OF THIS PAGE

UNCLASSFIED

UNCLASSFIED

Block 19 continued

Abstract

The simple and reliable single filament test methods for predicting the compressive properties of fibers are a must for development activities of fibers in laboratories because of difficulties in composite compression test methods. Therefore, in this study, two single filament compression test methods, which are elastic loop and bending beam test, are conducted for several polymeric fibers including Kevlars, PBO and PBZT and a few carbon fibers such as T-50 and P-75S, in order to obtain their compressive properties. Also the compressive failure modes of fibers, which occur as a kink band formation in polymeric fibers and as a fracture in carbon fibers are investigated. In addition, a FORTRAN program is written for numerical analysis of non-linear geometry elastica problems such as bending a single fiber with large displacements.

A comparison of results obtained in this study is made with the previous studies. It is found that generally the compressive strengths of the fibers obtained in this study are higher than the composite compression test results. The kink band formation in polymeric fibers were investigated thoroughly and it is concluded that the critical kink band formation represents the buckling of separated microfibrils due to elastic instability. Also the FORTRAN program is applied to measure the fiber compressive properties as new potential single filament test method.